Colloquium: Artificial gauge potentials for neutral atoms

Jean Dalibard[*] and Fabrice Gerbier[†]

Laboratoire Kastler Brossel, CNRS, UPMC, Ecole normale supérieure,
24 rue Lhomond, 75005, Paris, France

Gediminas Juzeliūnas[‡]

Institute of Theoretical Physics and Astronomy, Vilnius University,
A. Goštauto 12, Vilnius 01108, Lithuania

Patrik Öhberg[§]

SUPA, Department of Physics, Heriot-Watt University,
Edinburgh, EH14 4AS, United Kingdom

(published 30 November 2011)

When a neutral atom moves in a properly designed laser field, its center-of-mass motion may mimic the dynamics of a charged particle in a magnetic field, with the emergence of a Lorentz-like force. In this Colloquium the physical principles at the basis of this artificial (synthetic) magnetism are presented. The corresponding Aharonov-Bohm phase is related to the Berry's phase that emerges when the atom adiabatically follows one of the dressed states of the atom-laser interaction. Some manifestations of artificial magnetism for a cold quantum gas, in particular, in terms of vortex nucleation are discussed. The analysis is then generalized to the simulation of non-Abelian gauge potentials and some striking consequences are presented, such as the emergence of an effective spin-orbit coupling. Both the cases of bulk gases and discrete systems, where atoms are trapped in an optical lattice, are addressed.

CONTENTS

I. INTRODUCTION

In 1982 Feynman introduced the concept of a quantum emulator as a possibility to circumvent the difficulty of simulating quantum physics with classical computers (Feynman, 1982). His idea, based on the universality of quantum mechanics, was to use one controllable device to simulate other systems of interest. Nowadays Feynman's intuition is being implemented in various setups and among them cold gases of neutral atoms play a central role (Bloch, Dalibard, and Zwerger, 2008; Buluta and Nori, 2009). These gases constitute remarkably flexible playgrounds. They can be formed of bosons, fermions, or mixtures of both. Their environment can be controlled using the potential created by laser light, with harmonic, periodic, quasiperiodic, or disordered energy landscapes. Interactions between particles can be adjusted using scattering resonances. At first sight the only missing ingredient for implementing Feynman's idea with dilute atomic gases is the equivalent of orbital magnetism, which would allow one to simulate phenomena such as the quantum Hall effect. Here we discuss a general path that has recently emerged to fill this missing item, by using atom-light

[*]jean.dalibard@lkb.ens.fr
[†]fabrice.gerbier@lkb.ens.fr
[‡]Gediminas.Juzeliunas@tfai.vu.lt
[§]P.Ohberg@hw.ac.uk

interaction to generate artificial gauge potentials acting on neutral matter. The major part of this Colloquium addresses the case of a gauge field which has the U(1) Abelian symmetry, such as electromagnetism, but we also discuss more elaborate configurations leading to non-Abelian gauge potentials.

From the quantum mechanics point of view, the orbital magnetism of a particle with charge e can be viewed as a consequence of the Aharonov-Bohm phase γ acquired by the particle when it travels along a closed contour $\mathcal{C}$ (Aharonov and Bohm, 1959). This phase has a geometric origin and does not depend on the duration needed for completing the trajectory. It reads $\gamma = 2\pi\Phi/\Phi_0$, where Φ is the flux of the magnetic field through the contour $\mathcal{C}$ and $\Phi_0 = h/e$ is the flux quantum. Therefore, the quest for artificial magnetism is to realize situations where a neutral particle acquires a geometrical phase when it follows the contour $\mathcal{C}$. Similarly the generation of a non-Abelian field can be achieved for particles with an internal degree of freedom. After completion of the trajectory along $\mathcal{C}$, the initial internal state of the particle $|\psi_i\rangle$ is changed into $U|\psi_i\rangle$, where U is a unitary operator acting in the internal Hilbert space of the particle and depending only on the geometry of the contour. Note that throughout this Colloquium the artificial gauge potentials that appear are not dynamical variables, i.e., they are not influenced by the motion of the atoms.

One of the simplest examples of geometric phases, the so-called Berry's phase, plays a central role in this paper. It emerges, for example, when a neutral particle with magnetic moment $\boldsymbol{\mu}$ moves in a (real) nonhomogenous magnetic field $\boldsymbol{B}_0(\boldsymbol{r})$ (Berry, 1984). If the particle is prepared at a point $\boldsymbol{r}_0$ in one of the local eigenstates $|m(\boldsymbol{r}_0)\rangle$ of the Hamiltonian $-\boldsymbol{\mu} \cdot \boldsymbol{B}_0(\boldsymbol{r})$ and moves slowly enough, it follows adiabatically the local eigenstate $|m(\boldsymbol{r}_t)\rangle$. Once the trajectory along $\mathcal{C}$ is completed, the particle returns to the internal state $|m(\boldsymbol{r}_0)\rangle$, up to a phase factor containing a geometric component.

Berry's phase is also present in atom-light interactions (Dum and Olshanii, 1996). The role of the magnetic states $|m(\boldsymbol{r})\rangle$ is now played by the dressed states, i.e., the eigenstates of the atom-light coupling. The dressed states can vary on a short spatial scale (typically the wavelength of light) and the artificial gauge fields can be quite intense, in the sense that the geometric phase is large compared to 2π for a contour encircling a gas of realistic size. If the gas is superfluid, it will thus contain many vortices at equilibrium. The situation considered here should not be confused with phase-imprinting methods, which correspond to imposing a dynamical rather than a geometrical phase to the atomic wave function [see Andersen *et al.* (2006) and references therein]. In the latter case one acts on the atoms with a time-dependent atom-light coupling, and the spatial phase profile of the light beam is dynamically transferred to the atom cloud. Here by contrast we look for a time-independent Hamiltonian and require that its ground state has a nonzero vorticity.

The use of geometrical phases is not the only way to reach a Hamiltonian with an artificial gauge potential for neutral particles. Rotating the system at angular frequency Ω around a given axis (say z) also leads to artificial magnetism in the rotating frame, with $B_z \propto \Omega$. This has been widely used in the context of quantum gases

[see Cooper (2008) and Fetter (2009) for reviews], and it is well suited when the confining potential is rotationally invariant around the z axis. The Hamiltonian is then time independent in the rotating frame, and the standard formalism of equilibrium statistical physics is applicable. However, if the confining potential has a nonzero anisotropy in the laboratory frame, the Hamiltonian is time dependent in any frame and the situation is difficult to handle from a theoretical point of view. By contrast, methods based on geometrical phases do not impose any constraint on the symmetry properties of the initial Hamiltonian and the artificial gauge fields are produced in the laboratory frame. Together with the possibility to extend the scheme to non-Abelian gauge potentials, this represents a significant advantage. Of course, the use of laser beams also comes with some drawbacks that we address in this Colloquium, such as heating of the atoms because of residual spontaneous emission.

This Colloquium is organized as follows. In Sec. II we present a toy model, where the atomic transition that is coupled to the laser light is represented by a simple two-level system. It allows us to identify the important elements for the emergence of artificial gauge potentials: gradients of the phase of the light beam and of its intensity or detuning with respect to atomic resonance. This model is relevant for some atomic species such as ytterbium atoms that possess an electronic excited state with an extremely long lifetime, but it cannot be used as such for the alkali-metal atoms, which are the most commonly used species in experiments. Indeed the large rate of spontaneous emission processes and the ensuing random recoils of the atoms cause in this case a prohibitive heating of the gas. In Sec. III we thus turn to schemes where the ground state manifold is degenerate, first introduced by Dum and Olshanii (1996), and we show that a gauge potential with a nonvanishing curl can then be generated even if the population of the excited states is negligible (Juzeliūnas and Öhberg, 2004). We also discuss the recent implementation of an artificial magnetic field in a Bose-Einstein condensate of rubidium atoms by Lin, Compton, Jiménez-García *et al.* (2009), which led to the observation of quantized vortices. Section IV is devoted to the preparation of non-Abelian gauge fields and to the discussion of some of their physical consequences: negative refraction and reflection, implementation of the Klein paradox, and the non-Abelian Aharonov-Bohm effect. In Sec. V we study the production of artificial gauge potentials in optical lattices. Starting from the proposal by Jaksch and Zoller (2003), we show that one can reach the strong magnetic field regime, where the phase γ per lattice cell can take any value between 0 and 2π. We also briefly discuss the implementation of non-Abelian schemes in a lattice.

Throughout this Colloquium, we mostly address single atom physics, with some incursions to many-body physics at the mean-field level when dealing with the generation of quantized vortices in a superfluid. The application of a gauge field on a quantum gas can also lead to the emergence of strongly correlated many-body states. Their detailed discussion is outside the scope of this Colloquium, and we simply mention a few lines of research in this direction in the final Outlook section.

II. TOY MODEL: TWO-LEVEL ATOM IN A LIGHT BEAM

In order to present the essential ingredients of the physics of geometrical gauge fields, we start this Colloquium by discussing the simplest scheme for which artificial magnetism can occur. We consider a single quantum particle with a two-level internal structure, and we show how the adiabatic following of one particular internal state can provide the desired gauge fields. This will allow us to present with a minimum algebra the important physical concepts, which will subsequently be generalized to more complex schemes.

We denote $\{|g\rangle, |e\rangle\}$ a basis of the two-dimensional Hilbert space associated with the internal degree of freedom of the particle. Later on these states will represent electronically ground and excited states of an atom, respectively. We assume that the particle evolves in space-dependent external fields that couple $|g\rangle$ and $|e\rangle$. At the present stage we do not specify the physical origin of these fields. In practice these can be the fields of optical lasers, microwave fields, and/or static electric or magnetic fields acting on the electric or magnetic dipole moment of the particle. The general form for the Hamiltonian of the particle of mass M is

$$H = \left(\frac{P^2}{2M} + V\right)\hat{1} + U,\qquad(1)$$

where $P = -i\hbar\nabla$ is the momentum operator and $\hat{1}$ is the identity operator in the internal Hilbert space. The coupling operator U can be written in the matrix form

$$U = \frac{\hbar\Omega}{2}\begin{pmatrix}\cos\theta & e^{-i\phi}\sin\theta \\ e^{i\phi}\sin\theta & -\cos\theta\end{pmatrix}.\qquad(2)$$

The particle dynamics is determined by four real quantities that may all depend on the position vector r: The potential V acts on the particle in a way that is independent of its internal state, whereas the generalized Rabi frequency Ω characterizes the strength of the coupling that lifts the degeneracy between $|g\rangle$ and $|e\rangle$. The two remaining quantities are the mixing angle θ and the phase angle ϕ. For a two-level atom in a monochromatic laser field [see Eq. (10)], $\Omega\cos\theta$ stands for the laser detuning from the atomic resonance, $\Omega\sin\theta$ is the magnitude of the atom-laser coupling, and ϕ is the laser phase.

In this section we first describe the atomic dynamics when the internal state of the particle follows adiabatically one of the eigenstates of U, and we give the expression of the geometrical gauge potentials that appear in this case. Then we present a possible implementation of the Hamiltonian (1) and (2) with an alkaline-earth atom irradiated by a quasiresonant laser beam, and we discuss the physical origin of the gauge potentials. We also study under which condition the strength and the spatial extent of the geometric magnetic field are sufficient to induce a large circulation of the atomic phase. This can then allow for the nucleation of a lattice of quantized vortices if one applies this scheme to a collection of identical atoms forming a superfluid.

A. Adiabatic following of a dressed state

At a point r the eigenstates of the matrix U are

$$|\chi_1\rangle = \begin{pmatrix}\cos(\theta/2) \\ e^{i\phi}\sin(\theta/2)\end{pmatrix},$$
$$|\chi_2\rangle = \begin{pmatrix}-e^{-i\phi}\sin(\theta/2) \\ \cos(\theta/2)\end{pmatrix},\qquad(3)$$

with eigenvalues $\hbar\Omega/2$ and $-\hbar\Omega/2$, respectively. We call them *dressed states*, anticipating the following discussions where they will correspond to the local eigenstates of the Hamiltonian describing the coupling between an atom and a light field. Since the states $\{|\chi_j\rangle\}$ form a normalized, orthogonal basis, the quantity $i\langle\chi_j|\nabla\chi_j\rangle$ is a real number and the relation $\langle\nabla\chi_2|\chi_1\rangle = -\langle\chi_2|\nabla\chi_1\rangle$ holds, where we set $|\nabla\chi_j\rangle \equiv \nabla(|\chi_j\rangle)$.

Using the $\{|\chi_j\rangle\}$ basis for the internal Hilbert space, we can write the full state vector of the particle as

$$|\Psi(r, t)\rangle = \sum_{j=1,2}\psi_j(r, t)|\chi_j(r)\rangle.\qquad(4)$$

Suppose now that at an initial time the particle is prepared in one particular internal dressed state, say $|\chi_1\rangle$. If the velocity distribution of the particle involves only sufficiently small components, the internal state of the particle will remain proportional to $|\chi_1\rangle$ for all times. This is equivalent to the Born-Oppenheimer approximation in molecular physics: The position r of the particle and its internal degree of freedom play the role of the nuclear coordinates and of the electron dynamics, respectively.

We now derive the equation of motion for ψ_1 in the case where ψ_2 remains negligible at all times. We first consider the action of the momentum operator P on the full state vector $|\Psi\rangle$. Employing $\nabla[\psi_j|\chi_j\rangle] = [\nabla\psi_j]|\chi_j\rangle + \psi_j|\nabla\chi_j\rangle$ and the completeness relationship, one has

$$P|\Psi\rangle = \sum_{j,l=1}^{2}[(\delta_{j,l}P - A_{jl})\psi_l]|\chi_j\rangle,\qquad(5)$$

with $A_{jl}(r) = i\hbar\langle\chi_j|\nabla\chi_l\rangle$. Assuming that $\psi_2 = 0$, we project the Schrödinger equation $i\hbar|\dot{\Psi}\rangle = H|\Psi\rangle$ onto the internal dressed state $|\chi_1\rangle$, where H is the full Hamiltonian (1). This leads to a closed equation for the probability amplitude ψ_1 to find the atom in the first dressed state (Mead and Truhlar, 1979; Jackiw, 1988; Berry, 1989; Moody, Shapere, and Wilczek, 1989; Mead, 1992):

$$i\hbar\frac{\partial\psi_1}{\partial t} = \left[\frac{(P - A)^2}{2M} + V + \frac{\hbar\Omega}{2} + W\right]\psi_1.\qquad(6)$$

In addition to the terms V and $\hbar\Omega/2$ that were already explicit in the initial Hamiltonian (1), two geometric potentials A and W emerge in the adiabatic elimination of the state $|\chi_2\rangle$, due to the position dependence of the internal dressed states. The first one is the vector potential

$$A(r) = i\hbar\langle\chi_1|\nabla\chi_1\rangle = \frac{\hbar}{2}(\cos\theta - 1)\nabla\phi.\qquad(7)$$

The effective magnetic field associated with A is

$$B(r) = \nabla \times A = \frac{\hbar}{2}\nabla(\cos\theta) \times \nabla\phi.\qquad(8)$$

When this artificial magnetic field is nonzero, the vector potential A cannot be eliminated from Eq. (6) by a gauge transformation. The particle acquires an effective charge (that we set equal to 1 by convention) and its motion exhibits the usual features associated with orbital magnetism. A nonzero value of B occurs only if both the mixing angle θ and the phase angle ϕ vary in space with noncollinear gradients. The second geometrical potential appearing in Eq. (6) is the positive scalar term

$$W(\mathbf{r}) = \frac{\hbar^2}{2M}|\langle \chi_2 |\mathbf{\nabla}\chi_1\rangle|^2 = \frac{\hbar^2}{8M}[(\mathbf{\nabla}\theta)^2 + \sin^2\theta(\mathbf{\nabla}\phi)^2].$$
(9)

The first experimental evidence for the scalar potential in quantum optics was given by Dutta, Teo, and Raithel (1999). As such, the geometric scalar potential is not a very useful tool in the sense that there exist many other ways to create a scalar potential on atoms, using, for example, the ac Stark shift created by a far-detuned laser beam (Grimm, Weidemüller, and Ovchinnikov, 2000). However, in the following we estimate the value of the scalar potential for some relevant configurations, because it must be taken into account to determine the equilibrium shape of the cloud.

The contributions of the vector and scalar potentials in Eq. (6) can be recovered in a systematic expansion in terms of the dimensionless adiabatic parameter, defined as the ratio between the short and long time scales (Littlejohn and Weigert, 1993; Weigert and Littlejohn, 1993). The term $-\mathbf{P}\cdot\mathbf{A}/M$ appears at first order of the expansion, whereas $A^2/2M$ and the scalar potential W appear at second order. An extra term that is quadratic with respect to $\mathbf{P}$ also shows up at second order, with a contribution that can reach that of the scalar potential when $P^2/M \sim \hbar\Omega$. We will not address this extra term in this Colloquium, because (i) we are mostly interested in the physics arising from the leading term of the expansion $-\mathbf{P}\cdot\mathbf{A}/M$ and (ii) we are restricted to situations where the atomic kinetic energy is much smaller than $\hbar\Omega$.

The reason for which A, B and W are called "geometrical" is clear from Eqs. (7)–(9), which depend only on the spatial variation of the angles θ and ϕ, i.e., on the geometry of the coupling between $|g\rangle$ and $|e\rangle$, but not on the strength Ω of this coupling. Note that if we consider the adiabatic following of $|\chi_2\rangle$ instead of $|\chi_1\rangle$, the equation of motion for ψ_2 contains the same scalar potential W and the opposite vector potential $-A$.

B. Practical implementation with alkaline-earth atoms

We now discuss how the above model can be implemented in quantum optics, in order to create artificial orbital magnetism on a gas of cold neutral atoms (Dum and Olshanii, 1996; Visser and Nienhuis, 1998). The simplest scheme consists of shining a single laser beam on an atom. We restrict the internal atomic dynamics to a two-level transition of frequency ω_A, between the ground state $|g\rangle$ and an electronically excited state $|e\rangle$. The laser light of frequency ω_L is supposed to be close to resonance with this transition. We suppose that the rate of spontaneous emission of photons from the excited state $|e\rangle$ is negligible on the relevant time scale, which is a realistic assumption if the experiment is performed using the intercombination line of alkaline-earth
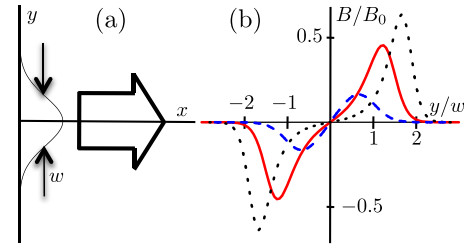

FIG. 1 (color online).   (a) A running wave propagating along the x axis, with a Gaussian profile along the y axis (waist w), is used to create a geometrical gauge field on a two-level atom whose resonance frequency is close to the laser frequency. (b) Variation of the amplitude of the artificial magnetic field B (in units of $B_0 = \hbar k/w$) as a function of y/w; $\kappa^{(0)}/\Delta = 1$ (dashed), 5 (solid), and 20 (dotted).

atoms (calcium or strontium) or ytterbium atoms. Indeed for these atomic species, the radiative lifetime of the excited state $|e\rangle$ involved in the intercombination line [also used in optical atomic clocks (Ye, Kimble, and Katori, 2008)] is several seconds or even tens of seconds, much larger than the typical duration of cold atom experiments.

We suppose that the atomic center-of-mass motion is restricted to the x-y plane using a suitable trapping potential that freezes the z degree of freedom. The mode of the laser beam is a Gaussian traveling wave of wave number k and wavelength $\lambda = 2\pi/k$ propagating along the x axis, with a waist w in the y direction [Fig. 1(a)]. The states $|g\rangle$ and $|e\rangle$ stand for eigenstates of the internal atomic Hamiltonian in the absence of coupling with the radiation field. Using the rotating wave approximation, the coupling matrix U can be written in the present case (Cohen-Tannoudji, Dupont-Roc, and Grynberg, 1992)

$$U = \frac{\hbar}{2}\begin{pmatrix} \Delta & \kappa^* \\ \kappa & -\Delta \end{pmatrix},$$
(10)

where the detuning $\Delta = \omega_L - \omega_A$, and where the Rabi frequency κ characterizes the strength of the atom-laser coupling. The spatially varying phase of the laser is incorporated into κ which is therefore complex.

In the following we neglect the diffraction of the laser beam and set $\kappa(\mathbf{r}) = \tilde{\kappa}(y)e^{ikx}$, where $\tilde{\kappa}$ is real and positive. The angle ϕ featured in Eq. (2) is then simply the running phase kx of the propagating laser beam and $\mathbf{\nabla}\phi = k\mathbf{e}_x$, where $\mathbf{e}_x$ is the unit vector in the x direction. The mixing angle θ is given by $\tan\theta = \tilde{\kappa}/\Delta$ and two options are available to provide a nonzero $\mathbf{\nabla}\theta$. One can use either a gradient of the Rabi frequency $\tilde{\kappa}$ produced by a spatial variation in the laser intensity or a gradient of the detuning Δ. In this section we discuss these two configurations, which we refer to as grad-κ and grad-Δ configurations, respectively.

1. Grad-κ configuration

A possible scheme leading to this configuration is shown in Fig. 1, where we take advantage of the transverse Gaussian profile of the laser beam. The Rabi frequency is $\tilde{\kappa}(y) = \kappa^{(0)}e^{-y^2/w^2}$, which leads to an effective magnetic field B that is parallel to the z axis, with the amplitude obtained using Eq. (8):

$$B = B_0 \frac{\Delta \tilde{\kappa}^2}{\Omega^3} \frac{y}{w}, \tag{11}$$

with $\Omega^2 = \Delta^2 + \tilde{\kappa}^2$. Here we set $B_0 = \hbar k / w$, which gives the typical scale for the effective magnetic field appearing in this case. The characteristic length scale associated with orbital magnetism is the so-called magnetic length $\ell_B = (h/B)^{1/2}$, which gives the size of the elementary quantum cyclotron orbit. We obtain in this context $\ell_B \sim (w\lambda)^{1/2}$ (hence $\ell_B > \lambda$) for $B \sim B_0$.

The variation of B with y/w is plotted in Fig. 1(b) for various values of the ratio $\kappa^{(0)}/\Delta$. When $\kappa^{(0)}/\Delta \gg 1$ the maximal value of B is obtained approximately at the point where $\tilde{\kappa} = \Delta$, i.e., $y_{max} \approx w[\log(\kappa^{(0)}/\Delta)]^{1/2} \gg w$ and $B_{max} \approx B_0 y_{max}/(2\sqrt{2}w)$. At first sight the limiting regime $\kappa^{(0)}/\Delta \to \infty$ is interesting since it leads to $B_{max} \to \infty$. However, the interval Δy over which B takes significant values tends to zero as $1/B_{max}$, and eventually becomes smaller than the magnetic length $\ell_B \propto 1/B_{max}^{1/2}$, making this regime $\kappa^{(0)} \gg \Delta$ not useful in practice. More generally we find that

$$\int_0^{+\infty} B\,dy = \frac{\hbar k}{2}\left[1 - \frac{1}{\sqrt{1 + (\kappa^{(0)}/\Delta)^2}}\right] < \frac{\hbar k}{2}. \tag{12}$$

Consider, for example, the case $\kappa^{(0)}/\Delta = 5$. The maximum value $B_{max} \approx 0.45 B_0$ is obtained for $|y|/w \approx 1.2$, and $B > B_0/4$ over an interval of width $\sim w/2$.

The calculation of the scalar potential leads to

$$W(y) = \frac{E_R}{4} \frac{\tilde{\kappa}^2(y)}{\Delta^2 + \tilde{\kappa}^2(y)}\left[1 + \frac{4y^2}{w^4 k^2} \frac{\Delta^2}{\Delta^2 + \tilde{\kappa}^2(y)}\right], \tag{13}$$

where we define the recoil energy $E_R = \hbar^2 k^2 / 2M$ as the kinetic energy of an atom initially at rest when it absorbs or emits a single photon. Realistic values of the waist w are such that $kw \gg 1$. When $\kappa^{(0)} \lesssim$ a few Δ, the main contribution to the scalar potential (9) is the $(\nabla \phi)^2$ term, which corresponds to the first term in the bracket of Eq. (13). The scalar potential then creates a potential bump that is maximal in $y = 0$, with a height scaling such as E_R. When $\kappa^{(0)}/\Delta \gg 1$, the contribution proportional to $(\nabla \theta)^2$ to the scalar potential becomes dominant [second term in the bracket of Eq. (13)]. The corresponding force is now large around the point y_{max} and may create strong distortions of the trapped atom cloud.

2. Grad-Δ configuration

We suppose now that the laser waist w is large, so that the spatial mode of the laser is well approximated by a plane wave and the Rabi frequency $\tilde{\kappa}$ can be taken uniform. We also assume that a gradient of detuning is present along the y axis, so that $\Delta = \Delta'(y - y_0)$. For alkaline-earth or ytterbium atoms, it can be created using an additional off-resonant laser, which produces a differential light shift for the g and e states. The effective magnetic field $\boldsymbol{B}$ is parallel to the z axis, with an amplitude given by

$$B = B_0 \mathcal{L}^{3/2}(y),$$
$$\mathcal{L}(y) = \frac{1}{1 + (y - y_0)^2/\ell_\kappa^2}, \tag{14}$$

where we introduced the characteristic length $\ell_\kappa = \tilde{\kappa}/|\Delta'|$ and set $B_0 = \hbar k/(2\ell_\kappa)$. The scalar potential is

$$W(y) = \frac{E_R}{4}\left(\mathcal{L}(y) + \frac{1}{k^2 \ell_\kappa^2} \mathcal{L}^2(y)\right). \tag{15}$$

The magnetic field can be made arbitrarily large by taking $\Delta' \to \infty$, but as for the grad-κ case this is not relevant in practice. Indeed the field then takes a large value only over a domain whose size $\ell_\kappa \propto 1/\Delta'$ becomes smaller than the magnetic length $\ell_B = (\ell_\kappa \lambda/2)^{1/2}$.

C. Validity of the adiabatic approximation

We now discuss the validity of the adiabatic approximation (Messiah, 1961b) underlying the projection mechanism generating the gauge potentials. For simplicity, we adopt a semiclassical point of view in which we classically treat the atomic center-of-mass motion, but still use quantum mechanics to describe its internal dynamics. The atom is supposed to be initially at rest in the internal state $|\chi_1\rangle$, and then accelerated in order to reach the velocity $\boldsymbol{v}$. The population Π_2 of the state $|\chi_2\rangle$ at the end of the acceleration process is not strictly zero. For small $|\boldsymbol{v}|$ it is given by $\Pi_2 \approx |\boldsymbol{v} \cdot \langle \chi_2 | \nabla \chi_1 \rangle / \Omega|^2$, where the motional coupling is $\langle \chi_2 | \nabla \chi_1 \rangle = [\nabla \theta - i \sin \theta \nabla \phi] e^{-i\phi}/2$ (Cheneau *et al.*, 2008).

We first address the grad-κ implementation discussed above, for which $\nabla \theta = \Delta \nabla \tilde{\kappa} / (\Delta^2 + \tilde{\kappa}^2)$, and we restrict to the practical case where $\kappa^{(0)} \lesssim$ a few Δ. Since the gradient of the laser intensity always occurs with the spatial scale $w \gg k^{-1}$, we find that $|\nabla \theta| \ll k$. The motional coupling is dominated by the contribution of $\nabla \phi$ and reaches the maximum value $|\langle \chi_2 | \nabla \chi_1 \rangle \approx k|\sin(\theta)| = k|\kappa^{(0)}/\Omega|$. Using the fact that the atomic velocity changes by an amount equal to the recoil velocity $v_R = \hbar k/M$ during each photon absorption or emission process, a necessary condition for the adiabatic approximation to hold ($\Pi_2 \ll 1$) is thus

$$\hbar\Omega \gg \sqrt{\hbar \kappa^{(0)} E_R}. \tag{16}$$

In most situations of practical interest, $\kappa^{(0)} \sim \Delta$ and Eq. (16) reduces to the intuitive condition

$$\hbar \kappa^{(0)} \gg E_R, \tag{17}$$

stating that the coupling strength should be much larger than the recoil energy. Of course, the validity condition for the adiabatic approximation is more stringent if the atomic velocity is notably larger than v_R.

We now address the case of the grad-Δ scheme. Far away from any resonance point where Δ vanishes, the adiabaticity condition (16) still holds. Near a resonance point, the validity condition for the adiabatic approximation may be more stringent, since the gradient of the mixing angle $|\nabla \theta| \sim 1/\ell_\kappa$ can be large. More precisely, suppose that on each side of the resonance point, $|\Delta|$ is large compared to the coupling $\tilde{\kappa}$. The dressed states then nearly coincide with the bare states, with either $\{|\chi_1\rangle = |e\rangle, |\chi_2\rangle = |g\rangle\}$ or $\{|\chi_1\rangle = |g\rangle, |\chi_2\rangle = |e\rangle\}$. The switch between these two configurations occurs within a region of size $\sim l_\kappa$ around the resonance point. Taking again the atomic velocity on the order of the recoil velocity v_R, the adiabatic condition reads

$$\hbar\tilde{\kappa} \frac{k\ell_\kappa}{[1 + (k\ell_\kappa)^2]^{1/2}} \gg E_R. \tag{18}$$

When $k\ell_\kappa \gg 1$, this reduces to Eq. (16) in $y = y_0$, i.e., $\hbar\tilde\kappa \gg E_R$. In the opposite limit $k\ell_\kappa \ll 1$, the peak value of B is very large, but it is reached only in a small region of width $\ell_\kappa \ll k^{-1}$ and the adiabaticity condition $\tilde\kappa\ell_\kappa \gg v_R$ is more demanding. This is thus not a convenient configuration for a continuum implementation, but it becomes relevant for the lattice case (Sec. V).

D. Physical interpretation of the geometric potentials

We now turn to the physical interpretation of the geometrical gauge fields. We focus our discussion on the two-level system of Secs. II.A and II.B, but the following physical images can be generalized to the schemes that are analyzed in the next sections.

The scalar potential W can be interpreted as the kinetic energy associated with the fast micromotion of the particle. This was first explained for a classical continuous internal degree of freedom by Aharonov and Stern (1992). Here we outline the reasoning of Cheneau *et al.* (2008) that addresses the case of a quantized internal degree of freedom. Consider a particle prepared in the internal state $|\chi_1\rangle$, with a center-of-mass state that consists of a wave packet localized around a given point r with a small extension compared to the scale of variation of θ and ϕ. We introduce the force operator $F = -\nabla U$ and note that the eigenstates $|\chi_j\rangle$ of the coupling U are not eigenstates of F. The force acting on the particle thus exhibits quantum fluctuations, $\langle F^2\rangle \neq \langle F\rangle^2$, which are characterized in the Heisenberg picture by the symmetrized correlation function

$$C(\tau) = \tfrac{1}{2}\langle \delta F(0) \cdot \delta F(\tau) + \delta F(\tau) \cdot \delta F(0)\rangle$$
$$= \hbar^2\Omega^2|\langle\chi_2|\nabla\chi_1\rangle|^2 \cos(\Omega\tau), \qquad (19)$$

with $\delta F(\tau) = F(\tau) - \langle F\rangle$. We now recall that in classical mechanics, a particle submitted to a rapidly oscillating force δF undergoes a micromotion with the average kinetic energy

$$E_K = \int \frac{\tilde C(\omega)}{2M\omega^2}\,d\omega, \qquad (20)$$

where $\tilde C(\omega)$ is the Fourier transform of $C(\tau)$. Inserting the value (19) of $C(\tau)$ into Eq. (20), we find that E_K coincides with the scalar geometric potential given in Eq. (9).

The vector potential A given in Eq. (7) is related to the Berry's phase γ that appears when a quantum system, here the two-state system associated with the internal degree of freedom of the particle, is slowly transported round a contour $\mathcal{C}$, while remaining in an eigenstate $|\chi(r)\rangle$ of its Hamiltonian (Berry, 1984):

$$\gamma(\mathcal{C}) = i\oint\langle\chi|\nabla\chi\rangle \cdot dr = \frac{1}{\hbar}\oint A \cdot dr, \qquad (21)$$

where the second equality holds for the two-level system considered above when it is prepared in the state $|\chi\rangle$.

When $B = \nabla \times A \neq 0$, the Lorentz force $F = v \times B$ acts on the atom when it moves with velocity v. For the scheme discussed in Sec. II.B, the momentum change imparted by the Lorentz force has a simple physical interpretation. Suppose that the atom moves along the y axis, with a trajectory starting from $y_1 \gg w$ at time t_1, and ending in $y_2 = 0$ at time t_2. Since B is directed along the z direction and v along the y direction, the average momentum change $\langle\Delta P\rangle$ is directed along x:

$$\langle\Delta P_x\rangle = -\int_{t_1}^{t_2} v_y(t)B\,dt = \int_0^{y_1} B\,dy. \qquad (22)$$

Using Eq. (12) and $y_1 \gg w$, we find that $\Delta P_x \approx \hbar k/2$ in the case where $\kappa^{(0)} \gg \Delta$. This result has a simple physical interpretation. When the atom is located in $y_1 \gg w$, the occupied dressed state is $\approx |g\rangle$. When the atom arrives at $y_2 = 0$ where the atom-laser coupling is maximal, the dressed state is $\approx (|g\rangle + |e\rangle e^{ikx})/\sqrt{2}$ in the limit $\kappa^{(0)} \gg \Delta$. Hence a measurement of the atomic momentum ΔP_x can give the results 0 or $\hbar k$, both with probability $\tfrac{1}{2}$, hence $\langle\Delta P_x\rangle = \hbar k/2$. A more detailed discussion of the physical origin of the Lorentz force for other atomic trajectories is given by Cheneau *et al.* (2008).

E. Achieving states with a nonzero circulation

After the discussion of some simple schemes that generate artificial gauge potentials, we turn to the effect of this potential on the external (center-of-mass) degree of freedom of the atom. One of the main motivations for the generation of artificial magnetic fields is indeed to create some extended regions where the orbital magnetism is sufficient to favor states with a nonzero circulation. For instance, if a superfluid is placed in such a region, its ground state will exhibit a vortex lattice. We now explore under which condition this can occur for the simple schemes outlined above.

When a charged superfluid (with $e = 1$ here by convention) is placed in a magnetic field, the vortex density is $\rho_v = B/(2\pi\hbar)$ or in other words $\rho_v = \ell_B^{-2}$, where ℓ_B is the magnetic length (Tinkham, 1996). If the magnetic field obtained from the geometric potential A keeps a value $\sim B$ on a disk of radius r, one therefore expects that $N_v \approx \pi r^2\rho_v = r^2 B/(2\hbar)$ vortices will be present in steady state in a superfluid filling this disk. We now determine whether one can reach a situation with $N_v \gg 1$, which is equivalent to requiring that the phase $\gamma(\mathcal{C})$ defined in Eq. (21) is large compared to 2π.

Consider again the grad-κ scheme represented in Fig. 1, where we choose, for example, $\kappa^{(0)} = 5\Delta$. In this way, one gets a fictitious magnetic field that is approximately uniform with a value $\sim B_0/4$ in the band parallel to the x axis, centered on $y = 1.2w$, with a width $\ell_y \approx w/2$. The length of this band along x is limited only by the diffraction of the laser beam, which occurs on a distance $\gg w$, if the waist w is chosen much larger than the laser wavelength $\lambda = 2\pi/k$. In order to study the physics of vortex lattices in this geometry, the requirement is thus simply to fit several vortex rows in the width ℓ_y. Since the distance between two vortex rows is $\approx \rho_v^{-1/2}$, this requirement can be written

$$N_{\text{vortex rows}} \approx \tfrac{1}{4}\sqrt{w/\lambda} \gg 1. \qquad (23)$$

Clearly this method is well adapted to the study of vortex lattices only if $w \gg \lambda$. The choice of a small waist (of the order of a few λ only) is not appropriate, because the scaling $B_0 \propto 1/w$, which would tend to favor small waists, is compensated by the other scaling $\ell_y \sim w$ over which the field keeps a significant value. A similar argument can be made for the grad-Δ scheme with $\ell_y = \ell_\kappa$.

So far we have restricted our discussion to the case of a single laser traveling wave and the spatial scale of variation for the mixing angle θ is thus the beam waist w. It is interesting to also consider the case where several traveling waves irradiate the atom at different angles, so that interference phenomena can introduce a much shorter length scale for θ, typically $\lambda/(2\pi)$. For simplicity we restrict ourselves to the case of two waves and we choose the corresponding wave vectors equal to $\boldsymbol{k}_\pm = k(\boldsymbol{e}_x \pm \boldsymbol{e}_y)/\sqrt{2}$. The resulting light field still has a spatially varying phase $\phi = kx/\sqrt{2}$, and it presents an interference pattern along the y direction with a spatial period $\lambda/\sqrt{2}$. Hence $|\boldsymbol{\nabla}\phi| \sim |\boldsymbol{\nabla}\theta| \sim k/\sqrt{2}$, and we find using Eq. (8) that the maximal modulus of the artificial magnetic field is $|B| \sim 0.1\hbar k^2 \kappa^{(0)}/\Delta$. This field is directed along the z axis and is a periodic function of y with changes of sign every $\lambda/(2\sqrt{2})$. The same reasoning as above shows that one can marginally localize one quantum of circulation in each disk of area k^{-2} over which the field is approximately uniform. In order to obtain a circulation $\gg 2\pi$, one needs to rectify this spatially alternating field. Practical solutions will be detailed in Sec. V devoted to artificial gauge fields in optical lattices.

III. GAUGE POTENTIALS FOR MULTILEVEL SYSTEMS

In the model discussed in Sec. II, the internal state of the atom is at any place a linear combination of ground and excited states, and each of these two states must have a relatively large weight in order to obtain a non-negligible artificial gauge potential. Therefore, this configuration can be used only if the excited electronic state has a very long radiative lifetime, as is the case for alkaline-earth species. In order to address a larger class of atoms (including the more widely used alkali atoms), we now turn to schemes that take advantage of the (quasi)degeneracy of the electronic ground level. Denoting $\{|g_j\rangle, j = 1, \ldots, N\}$ a basis set of the ground state manifold, we look for configurations where some dressed states are linear combinations of the $|g_j\rangle$ states, with a negligible contribution of the excited state manifolds, $|\chi\rangle \approx \sum_j \alpha_j |g_j\rangle$. As we will see, this can be obtained by taking benefit of a so-called *dark state* (Arimondo, 1996), or by choosing a laser frequency that is strongly detuned with respect to the atomic resonance lines. If the atom is prepared in such a dressed state and moves sufficiently slowly to follow it adiabatically, geometrical gauge potentials show up as in Sec. II.B (Dum and Olshanii, 1996). Since we use laser beams to provide the relevant stimulated Raman couplings between the states $|g_j\rangle$, the α_j coefficients can vary significantly on a short length scale, typically an optical wavelength. One can thus produce geometrical fields with comparable amplitudes to those found in Sec. II, while avoiding the strong heating that would be caused by spontaneous emission processes.

In this section we first consider the dark state case, which occurs for a Λ-level scheme, where two sublevels of the electronic ground states $|g_1\rangle$ and $|g_2\rangle$ are coupled to a single excited state $|e\rangle$ by two laser beams. The dark state is an eigenstate of the atom-laser coupling that is a linear combination of $|g_1\rangle$ and $|g_2\rangle$ with a strictly zero contribution of the excited state. We then discuss two possible practical implementations of this dark state scheme, first using laser beams

carrying orbital angular momentum, and then using counter-propagating Gaussian beams with a spatial shift of their axis. Finally we describe an alternative scheme involving a position-dependent detuning. This scheme that is not relying on dark states but on a large detuning has led to the first experimental observation by Lin, Compton, Jiménez-García *et al.* (2009) of a geometric magnetic field in the context of cold atom physics.

A. Artificial magnetic field in a Λ scheme

We consider the Λ-type atomic level structure represented in Fig. 2, where two laser beams couple the atomic states $|g_1\rangle$ and $|g_2\rangle$ to the third one $|e\rangle$. The lasers are tuned symmetric with respect to the average of the frequencies of the $g_1 - e$ and $g_2 - e$ transitions. The full atomic Hamiltonian is given in Eq. (1), and the coupling operator between the light and the atom written in the $\{|g_1\rangle, |e\rangle, |g_2\rangle\}$ basis reads using the rotating wave approximation

$$U = \frac{\hbar}{2}\begin{pmatrix} -2\delta & \kappa_1^* & 0 \\ \kappa_1 & 0 & \kappa_2 \\ 0 & \kappa_2^* & 2\delta \end{pmatrix}. \tag{24}$$

Here $\kappa_{1,2}$ are the complex, space-dependent Rabi frequencies, which include the spatially varying phases of the laser beams as in Sec. II.B. The frequency 2δ is the detuning of the two-photon excitation with respect to the Raman resonance between g_1 and g_2.

Suppose that the two-photon (Raman) excitation is resonant ($\delta = 0$). In this case the coupling matrix U possesses an eigenstate with zero energy called *dark* (or *uncoupled*). This state contains no contribution from the excited state $|e\rangle$ and reads

$$|D\rangle = (\kappa_2|g_1\rangle - \kappa_1|g_2\rangle)/\kappa, \tag{25}$$

where $\kappa = (|\kappa_1|^2 + |\kappa_2|^2)^{1/2}$. The two other eigenstates of U have the eigenenergies $\pm\hbar\kappa/2$, and read $|\pm\rangle = (|B\rangle \pm |e\rangle)/\sqrt{2}$, where $|B\rangle$ is the *bright* (coupled) state

$$|B\rangle = (\kappa_1^*|g_1\rangle + \kappa_2^*|g_2\rangle)/\kappa. \tag{26}$$

Dark states are frequently encountered in quantum optics applications such as subrecoil cooling (Aspect *et al.*, 1988), electromagnetically induced transparency (Arimondo, 1996; Harris, 1997; Lukin, 2003; Fleischhauer, Imamoglu, and
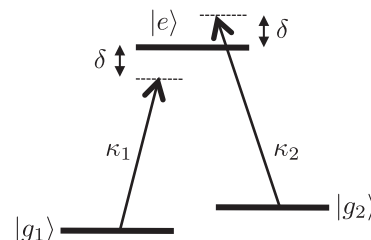
FIG. 2. Atomic Λ-level structure providing a dark state that depends parametrically on the Rabi frequencies κ_1 and κ_2.

Marangos, 2005) and stimulated Raman adiabatic passage (STIRAP) (Bergmann, Theuer, and Shore, 1998; Vitanov *et al.*, 2001; Král, Thanopulos, and Shapiro, 2007). These applications rely on the robustness of the state $|D\rangle$ with respect to the decoherence caused by spontaneous emission.

As in Sec. II, the full atomic state vector can be cast into the eigenstates of the operator U as

$$|\Psi(\mathbf{r})\rangle = \sum_{X=D,\pm} \psi_X(\mathbf{r})|X(\mathbf{r})\rangle, \qquad (27)$$

where the wave functions $\psi_D(\mathbf{r})$ and $\psi_\pm(\mathbf{r})$ describe the translational motion of an atom in the internal states $|D(\mathbf{r})\rangle$ and $|\pm(\mathbf{r})\rangle$, respectively. The adiabatic approximation assumes that the atom stays in the dark state, so that one can write $|\Psi(\mathbf{r})\rangle \approx \psi_D(\mathbf{r})|D(\mathbf{r})\rangle$. Projecting the Schrödinger equation onto the dark state and neglecting the couplings to the two other internal states $|\pm\rangle$, we arrive at an equation of motion for the dark state wave function $\psi_D(\mathbf{r})$ similar to Eq. (6):

$$i\hbar \frac{\partial \psi_D}{\partial t} = \left[\frac{(\mathbf{P} - \mathbf{A})^2}{2M} + V + W \right] \psi_D, \qquad (28)$$

where $\mathbf{A} = i\hbar\langle D|\boldsymbol{\nabla}D\rangle$ and $W = \hbar^2|\langle B|\boldsymbol{\nabla}D\rangle|^2/(2M)$ are the effective vector and scalar potentials emerging due to the spatial dependence of the dark state.

We, therefore, recover a situation similar to that of Sec. II.A, provided we replace $|\chi_1\rangle$ by $|D\rangle$ and $|\chi_2\rangle$ by $|B\rangle$. Comparing Eqs. (3) and (25), we set

$$\sqrt{\zeta} \equiv \frac{|\kappa_1|}{|\kappa_2|} = -\tan\frac{\theta}{2}, \qquad \phi_1 - \phi_2 = \phi, \qquad (29)$$

where the ϕ_j are the phases of the Rabi frequencies $\kappa_j = \tilde{\kappa}_j e^{i\phi_j}$ ($j = 1, 2$). The artificial magnetic field $\mathbf{B} = \boldsymbol{\nabla} \times \mathbf{A}$ given in Eq. (8) can be expressed in terms of ζ and ϕ:

$$\mathbf{B} = \hbar \frac{\boldsymbol{\nabla}\phi \times \boldsymbol{\nabla}\zeta}{(1 + \zeta)^2}. \qquad (30)$$

This effective magnetic field $\mathbf{B}$ is nonzero only if the gradients of the intensity ratio ζ and the relative phase ϕ are both nonzero and not parallel to each other. We discuss in the next sections some practical implementations of this Λ scheme, using either light beams with orbital angular momentum or counterpropagating Gaussian beams with an axis offset.

B. Using light beams with orbital angular momentum

We consider here the situation where the atoms located in the plane $z = 0$ are irradiated by two laser beams propagating along the z axis (see Fig. 3). The beams are prepared in Laguerre-Gauss modes, and they carry the orbital angular momenta $\hbar\ell_1$ and $\hbar\ell_2$ per photon. This scheme was first proposed by Juzeliūnas and Öhberg (2004) [see also Juzeliūnas *et al.* (2005), Juzeliūnas, Ruseckas, and Öhberg (2005), and Zhang, Li, and Sun (2005)]. The complex Rabi frequencies can be written $\kappa_j(\mathbf{r}) = \tilde{\kappa}_j(\rho)e^{i\ell_j\varphi}$ ($j = 1, 2$), where φ is the azimuthal angle around the z axis and ρ is the radial coordinate in the x-y plane. The effective magnetic field (30) is directed along the z direction and its amplitude reads

$$B(\rho) = \frac{\hbar\ell}{\rho} \frac{\partial_\rho\zeta}{(1 + \zeta)^2}, \qquad (31)$$
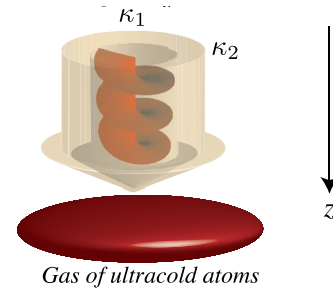

FIG. 3 (color online).   Two copropagating Gaussian beams, one of them being prepared in a Laguerre-Gauss mode with a nonzero orbital angular momentum, drive the two transitions of an atom with a Λ-level scheme. For an atom prepared in the dark state $|D\rangle$ [Eq. (25)], the nontrivial phase and intensity ratios between the Rabi frequencies κ_1 and κ_2 produce an artificial magnetic field parallel to the beam propagation axis.

where $\ell = \ell_1 - \ell_2$ is the relative winding number of the two beams.

For concreteness we consider beams with equal waists w and we choose $\ell_1 = \ell$, $\ell_2 = 0$ so that

$$\begin{aligned} \tilde{\kappa}_1(\rho) &= \kappa^{(0)}\rho^\ell e^{-\rho^2/w^2}, \\ \tilde{\kappa}_2(\rho) &= \kappa^{(0)}\rho_c^\ell e^{-\rho^2/w^2}, \end{aligned} \qquad (32)$$

where ρ_c is the radius at which the two beams have equal intensities. The winding number ℓ determines the shape of the gauge potentials. (i) For $\ell > 1$, the effective magnetic field is zero at the center of the beams and is maximum at $\rho = \rho_c[(\ell - 1)/(\ell + 1)]^{1/2\ell}$. (ii) For $\ell = 1$, the effective magnetic field is maximum at the origin with the value $B(0) = 2\hbar/\rho_c^2$. Its amplitude is inversely proportional to ρ_c, and can thus be controlled by changing the intensity ratio of the laser beams. Typically ρ_c has the same order of magnitude as the waist w. Since $w \gg k^{-1}$, the magnetic field generated in this way is notably smaller than the value $B_0 \approx \hbar k/w$ found in Sec. II.B, where we took advantage of the rapid spatial variation of the phase kx of a plane running wave.

The effective magnetic flux (in units of the Planck constant h) through a circle $\mathcal{C}$ of radius r_0 reads [see Eq. (21)]

$$\frac{\gamma(\mathcal{C})}{2\pi} = \frac{1}{h} \oint \mathbf{A} \cdot d\mathbf{l} = \ell \frac{\zeta_0}{1 + \zeta_0}, \qquad (33)$$

where ζ_0 is the intensity ratio at radius $\rho = r_0$. As explained in Sec. II.E, this flux gives the maximal number of vortices that can be observed if a superfluid gas is placed in this laser configuration. Its maximal value is ℓ and it is approximately reached for $\zeta_0 \gg 1$, i.e., for radii ρ_0 such that the intensity of beam 1 (with orbital angular momentum) largely exceeds that of beam 2 (with no angular momentum). In practice the winding number ℓ can reach a few tens (Hadzibabic, 2011); this configuration is therefore better suited to generate small vortex patterns rather than large vortex arrays.

C. Using spatially shifted laser beams

We now turn to the scheme represented in Fig. 4, which constitutes a direct generalization of the configuration studied in Sec. II.B for a two-level atom. It uses two Gaussian beams that are counterpropagating along the x axis, so that the phase
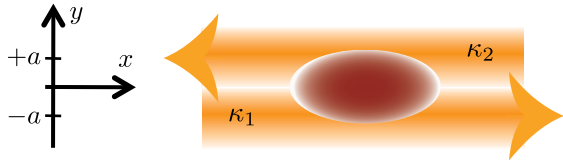
FIG. 4 (color online). Two counterpropagating beams with an offset $2a$ between their propagation axes drive the two transitions of an atom with a Λ-level scheme. With the atom prepared in the dark state $|D\rangle$, the laser beams induce an artificial magnetic field perpendicular to the figure plane.

difference between the two beams provides the necessary gradient of the phase angle ϕ entering in Eq. (30). The gradient of the intensity ratio ζ is obtained by a spatial shift $\pm a$ of each beam axis along the y direction. This configuration was first proposed by Juzeliūnas *et al.* (2006), and a modified version that is more flexible in terms of choice of laser polarizations was later suggested by Günter *et al.* (2009). It offers the possibility to reach large magnetic field values over an extended region of space, while taking advantage of the dark state configuration to minimize the spontaneous emission rate. This configuration with spatially shifted laser beams can also be used to generate the spin-Hall effect (Zhu *et al.*, 2006) and the Stern-Gerlach effect for chiral molecules (Li, Bruder, and Sun, 2007).

To simplify the mathematical treatment we assume that both beams have equal waists w and equal central Rabi frequency $\kappa^{(0)}$, and we neglect their diffraction along the x axis. Furthermore, we use the fact that the frequencies of the transitions $g_1 - e$ and $g_2 - e$ are very close in practice and we set $k_1 = k_2 = k$. The complex Rabi frequencies are then given by

$$\kappa_j(\boldsymbol{r}) = \kappa^{(0)} e^{\pm ikx} e^{-(y \pm a)^2 / w^2}, \qquad (34)$$

where the $+$ ($-$) sign stands for $j = 1$ ($j = 2$). The relative phase between the two beams is $\phi = 2kx$, and the intensity ratio reads $\zeta = \exp(8ya/w^2)$. The effective magnetic field is oriented along the z direction and its amplitude is obtained from Eq. (30):

$$B(y) = \frac{4\hbar ka}{w^2} \frac{1}{\cosh^2(4ya/w^2)}. \qquad (35)$$

The offset a of the beams along the y axis is *a priori* arbitrary. In practice, one should not take $a \gg w$, in order to keep a significant laser intensity along the line $y = 0$ where B is maximum, and ensure that the atoms adiabatically follow the dark state $|D\rangle$ at this location. Taking as a typical value $a = w/2$ we find $B(0) = 2\hbar k/w$, which is comparable to the result of Sec. II.B. Therefore, the conclusions of Sec. II.E concerning the possibility of generating large vortex arrays remain valid for this configuration. Similar to the geometric magnetic field $B(y)$, the scalar potential $W(y)$ is maximum along the line $y = 0$. An extra trapping potential V is therefore needed to prevent the atoms from flying away from this area.

D. Gauge potentials involving a gradient of detuning

We explained in Sec. II.B that the necessary gradient of the mixing angle θ can be provided by a gradient of the detuning

of the laser frequency, as well as by a gradient of the laser intensity. The same distinction applies to the Λ scheme and more generally to schemes involving multiple atomic levels. The first observation of a geometrical magnetic field by Lin, Compton, Jiménez-García *et al.* (2009) was actually based on a gradient of detuning for optical Raman transitions occurring between various ground sublevels. In this section we present the main features of this experiment and connect it with the already discussed configurations.

The experiment by Lin, Compton, Jiménez-García *et al.* (2009) was performed with ^{87}Rb atoms in their $F = 1$ hyperfine level. In the process all three Zeeman sublevels $|m_F\rangle$ with $m_F = 0, \pm 1$ acquire a significant population. The atoms are irradiated by two laser beams with wave vectors $\boldsymbol{k}_1$ and $\boldsymbol{k}_2$ that create a quasiresonant Raman coupling between Zeeman sublevels with $\Delta m_F = \pm 1$ (see Fig. 5 for details). The coupling occurs via the absorption of a photon in one beam and the stimulated emission of a photon in the other beam, accompanied by a change of the atom momentum of $\pm \hbar k_d$, where the difference of wave vectors $\boldsymbol{k}_d = \boldsymbol{k}_1 - \boldsymbol{k}_2 = k_d \boldsymbol{e}_x$ is chosen along x. An important ingredient is the application of a real magnetic field in addition to the laser beams. The Zeeman shift created by the magnetic field lifts the initial degeneracy of the sublevels $m_F = 0, \pm 1$. It gives a control knob on the two-photon detuning δ. In the initial experiment by Lin, Compton, Perry *et al.* (2009) a spatially uniform real magnetic field was applied, and it led to a spatially uniform vector potential, corresponding to a zero geometric magnetic field. Subsequently Lin, Compton, Jiménez-García *et al.* (2009) used a nonhomogeneous real magnetic field, making the two-photon detuning δ position dependent. In the following we assume the linear form $\delta = \delta'(y - y_0)$, where $\delta' > 0$ is the uniform gradient of detuning.
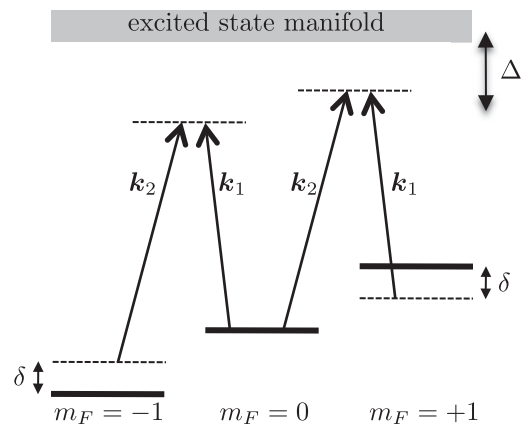

FIG. 5. Atomic scheme used by Lin, Compton, Jiménez-García *et al.* (2009). ^{87}Rb atoms with a spin $F = 1$ ground state are placed in an external magnetic field that displaces the sublevels $|m_F = \pm 1\rangle$ (dotted lines) with respect to $|m_F = 0\rangle$. The atoms are irradiated by two laser beams of wave vectors $\boldsymbol{k}_1$ and $\boldsymbol{k}_2$ that induce a resonant coupling between Zeeman sublevels satisfying $\Delta m_F = \pm 1$. An additional spatial gradient of the external magnetic field induces an additional displacement of the $|m_F = \pm 1\rangle$ sublevels (full lines). It thus creates a spatially varying two-photon detuning δ which allows one to generate an artificial gauge potential. Note that the frequency scale is not respected in the drawing (in practice $\Delta \gg \delta$).

This experiment can first be analyzed using the adiabatic framework used thus far. We assume that the coupling lasers can be considered as plane waves on the scale of the atomic cloud, so that the problem is translationally invariant along x. Therefore, the two-photon coupling κ induced by the laser pair can be written as $\kappa = \kappa^{(0)} e^{i\phi}$, with $\phi = \mathbf{k}_d \cdot \mathbf{r} = k_d x$ being the phase of the Raman coupling. The single-photon detuning Δ with respect to the excited state manifold involved in the transition is supposed to be very large compared to the Rabi frequencies. One can then perform an adiabatic elimination of the excited states to obtain an effective Hamiltonian acting on the ground state manifold. Keeping only the terms relevant for the subsequent discussion, this coupling written in the basis $\{|m_F = -1\rangle, |m_F = 0\rangle, |m_F = +1\rangle\}$ has the form of Eq. (24) with $\kappa_2 = \kappa_1^* = \kappa$.

We focus on the eigenstate of U associated with the lowest eigenvalue $-\hbar[\delta^2 + (\kappa^{(0)})^2/2]^{1/2}$,

$$|\chi\rangle = e^{i\phi}\cos^2\frac{\theta}{2}|-1\rangle - \frac{\sin\theta}{\sqrt{2}}|0\rangle + e^{-i\phi}\sin^2\frac{\theta}{2}|+1\rangle,$$

(36)

where we set $\tan\theta = \kappa^{(0)}/\sqrt{2}\delta$. The vector potential is now given by $\mathbf{A} = i\hbar\langle\chi|\nabla\chi\rangle = -\hbar\mathbf{k}_d\cos\theta$. The artificial magnetic field can be written in a form that is reminiscent of the result for the grad-Δ case of Sec. II.B [see Eq. (14)] (subject to the replacement of Δ by δ):

$$\mathbf{B} = \mathbf{e}_z B_0 \mathcal{L}^{3/2}(y - y_0),$$

(37)

where the characteristic length entering in the Lorentzian function $\mathcal{L}$ is $\ell_\kappa = \kappa^{(0)}/\sqrt{2}\delta'$, and where the peak value of the artificial magnetic field is $B_0 = \hbar k_d/\ell_\kappa$. The prediction (37) is in good agreement with the experimental results of Lin, Compton, Jiménez-García *et al.* (2009) ($\ell_\kappa \approx 40\lambda$ in the experiment). The scalar potential also takes a form that is similar to the one found for a two-level atom in the grad-Δ case: $W(y) \approx (\hbar^2 k_d^2/4M)\mathcal{L}(y - y_0)$, where we assumed $k_d\ell_\kappa \gg 1$. For an external trapping potential centered in y_0, $W(y)$ weakens the confinement along the y direction by creating in the vicinity of y_0 the antitrapping potential $-M\omega_W^2(y - y_0)^2/2$, with $\omega_W = \hbar k_d/\sqrt{2}M\ell_\kappa$ [$\omega_W/2\pi \simeq 30$ Hz for the parameters of Lin, Compton, Jiménez-García *et al.* (2009)].

Alternatively, the scheme described above can be analyzed using an original framework introduced by Spielman (2009). This framework is usable in the particular case where the only x dependence of the atom-laser coupling is the phase term $e^{\pm ik_d x}$, and it has then a larger range of validity than the standard adiabatic approximation. In a first step one "freezes" the y motion and diagonalizes exactly the x-dependent Hamiltonian $H_x = P_x^2/(2M) + U$, where U is the 3×3 matrix given in Eq. (24) with $\kappa_2 = \kappa_1^* = \kappa^{(0)} e^{ik_d x}$. The eigenstates are three-component spinors that can be labeled by their momentum $\hbar K_x$. For each K_x, this diagonalization yields three dispersion relations $E_n(K_x)$ ($n = 1, 2, 3$), each with a minimum at a momentum $K_{n,\min}$ depending on the two-photon detuning δ and Rabi frequency $\kappa^{(0)}$. At low energy and large coupling strength one obtains $E_n \approx \hbar^2(K_x - K_{n,\min})^2/2M^*$, where M^* is an effective mass. In a second step, one considers the motion along y and takes into

account the spatial variation of the detuning $\delta = \delta'(y - y_0)$. For the lowest energy state $n = 1$, this motion is described in an approximate manner by the projected Hamiltonian $H = P_y^2/(2M) + E_1$, which leads to the identification of an effective vector potential $\mathbf{A} = \hbar K_{1,\min}\mathbf{e}_x$. The spatial dependence of δ, hence of $K_{1,\min}$, along the y axis corresponds to an effective magnetic field $\mathbf{B} = \hbar(\partial K_{1,\min}/\partial y)\mathbf{e}_z$, described here in the Landau gauge. The exact diagonalization and adiabatic approaches agree when the latter is valid (see Sec. II.C), with $M^* \approx M$, in particular. For Rabi frequencies smaller than those required for the adiabatic approximation [see Eq. (17)], novel features appear in the exact diagonalization approach such as the possibility to simulate a spin-orbit coupling between two Bose-Einstein condensates in different dressed atomic states, experimentally observed by Lin, Jiménez-García, and Spielman (2011).

The discussion of Sec. II.E about the observable vortex pattern applies directly to the present scheme. The number of vortex rows that can fit along the y axis is again given by $\sim \ell_\kappa \sqrt{\rho_v} \sim \sqrt{\ell_\kappa/\lambda}$. The limit of large vortex arrays can thus in principle be reached with this configuration, provided one uses a relatively small gradient of detuning. Lin, Compton, Jiménez-García *et al.* (2009) generated about ten vortices in a rubidium Bose-Einstein condensate. These vortices did not order into a regular lattice, presumably because of the heating of the cloud and atom losses ($1/e$ lifetime of 1.4 s) caused by the residual photon scattering.

One could think that increasing the detuning of the laser coupling would solve the photon scattering problem. Unfortunately the situation is not so favorable, at least for alkali-metal species. Indeed, in contrast to the scalar light shift that scales as $U_{\rm scal} \propto I/\Delta$, where I is the light intensity, the two-photon Raman coupling κ is proportional to the vector part of the light shift $U_{\rm vec} \propto I\Delta_{\rm FS}/\Delta^2$. Here $\Delta_{\rm FS}$ denotes the fine structure splitting, which is only a few percent of ω_A for alkali atoms (2% for rubidium atoms, 5% for cesium atoms), and the above scaling for κ is valid for $\Delta_{\rm FS} \lesssim \Delta$. Therefore, in the limit of large detunings the Raman coupling κ decreases with Δ as fast as the photon scattering rate $\propto I\Gamma/\Delta^2$. In other words, the usual trick that consists of increasing both Δ and I to enhance the role of the scalar light shift with respect to spontaneous emission processes is not applicable in this context.

IV. NON-ABELIAN GAUGE POTENTIALS

The idea of non-Abelian geometric gauge potentials goes back to the work by Wilczek and Zee (1984), who considered the generalization of the adiabatic theorem to the case where the Hamiltonian of the system of interest possesses a group of eigenstates that remain degenerate (or quasidegenerate) and well isolated from other levels in the course of the time evolution. This analysis was followed by applications to many areas including *inter alia* molecular and condensed matter physics (Bohm *et al.*, 2003; Xiao, Chang, and Niu, 2010). In particular, the possibility of generating non-Abelian magnetic monopoles was demonstrated in the rotational dynamics of diatomic molecules (Moody, Shapere, and Wilczek, 1986; Zygelman, 1987, 1990; Bohm *et al.*, 1992) and in nuclear quadrupole resonance (Zee, 1988).
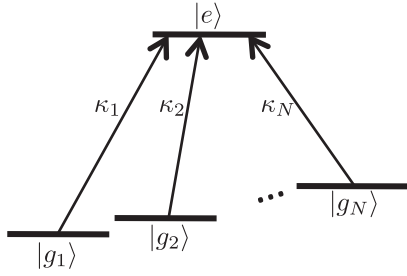
FIG. 6. Multipod configuration. An atomic state $|e\rangle$ is coupled to N different atomic states $|g_j\rangle$ ($j = 1, \ldots, N$) by N resonant laser fields.

In this section we are interested in the non-Abelian dynamics of cold atoms in light fields, which can emerge when a $(N + 1)$-state atomic system with $N \geq 3$ (see Fig. 6) is excited by a suitable configuration of laser beams. The first study in this direction was performed in the context of STIRAP by Unanyan *et al.* (1998) and Unanyan, Shore, and Bergmann (1999), who considered the behavior of a four-state atomic system (tripod configuration) when it is driven by three successive laser pulses. Subsequently, Osterloh *et al.* (2005) and Ruseckas *et al.* (2005) transposed the concept of gauge potentials to the case of a continuous atom-laser excitation relevant for the present review and identified situations where the non-Abelian gauge potentials emerge.

We start this section by providing a general formulation of the adiabatic motion of atoms when some internal atomic states remain degenerate in the presence of the atom-light coupling. We show how non-Abelian gauge potentials appear and discuss the structure of these potentials for some typical laser configurations. We also present some physical phenomena that are associated with non-Abelian gauge potentials, such as the generation of magnetic monopoles, Rashba spin-orbit coupling, and the non-Abelian Aharonov-Bohm effect.

A. Emergence of non-Abelian gauge potentials

In this section we consider atoms with $N + 1$ internal levels, which are coupled to a light field. We assume that we can cast the atom-laser interaction at any given point $\boldsymbol{r}$ as a time-independent $(N + 1) \times (N + 1)$ matrix $U(\boldsymbol{r})$ using the rotating wave approximation. Our starting point is then still the full atomic Hamiltonian of Eq. (1). For a fixed position $\boldsymbol{r}$, $U(\boldsymbol{r})$ can be diagonalized to give a set of $N + 1$ dressed states $|\chi_n(\boldsymbol{r})\rangle$, with eigenvalues $\varepsilon_n(\boldsymbol{r})$ ($n = 1, \ldots, N + 1$). The key feature that leads to non-Abelian gauge potentials is that some dressed states form a degenerate (or nearly degenerate) manifold, at any point $\boldsymbol{r}$ in space. More specifically we assume that the first q atomic dressed states form a degenerate subspace $\mathcal{E}_q$, and these levels are well separated from the remaining ones.

The full quantum state of the atom describing both internal and motional degrees of freedom can be written as $|\Psi\rangle = \sum_{n=1}^{N+1} \psi_n(\boldsymbol{r})|\chi_n(\boldsymbol{r})\rangle$, where each ψ_n is the wave function for the center-of-mass motion of the atom in the internal state $|\chi_n\rangle$. We are interested here in the dynamics of the atom when

it is initially prepared in the subspace $\mathcal{E}_q$. Neglecting transitions to states outside $\mathcal{E}_q$, we can project the full Schrödinger equation onto $\mathcal{E}_q$, and we arrive at a closed Schrödinger equation for the reduced column vector $\tilde{\Psi} = (\psi_1, \ldots, \psi_q)^\top$:

$$i\hbar \frac{\partial \tilde{\Psi}}{\partial t} = \left[\frac{(\boldsymbol{P} - \boldsymbol{A})^2}{2M} + V\hat{1}_q + \boldsymbol{\varepsilon} + W \right]\tilde{\Psi}, \tag{38}$$

where $\hat{1}_q$ is the identity matrix in $\mathcal{E}_q$ and $\varepsilon(\boldsymbol{r})$ is a diagonal matrix of eigenenergies $\varepsilon_n(\boldsymbol{r})$ ($n = 1, \ldots, q$). This equation is reminiscent of Eq. (6); however, $\boldsymbol{A}$ and W are now $q \times q$ matrices with the elements

$$A_{n,m} = i\hbar\langle\chi_n(\boldsymbol{r})|\nabla\chi_m(\boldsymbol{r})\rangle, \tag{39}$$

$$W_{n,m} = \frac{1}{2M} \sum_{l=q+1}^{N+1} \boldsymbol{A}_{n,l} \cdot \boldsymbol{A}_{l,m}, \tag{40}$$

with $n, m \in (1, \ldots, q)$. The effective vector potential $\boldsymbol{A}$ is called the Mead-Berry connection.

The effective magnetic field (or *curvature*) $\boldsymbol{B}$ associated with $\boldsymbol{A}$ is

$$B_i = \frac{1}{2}\epsilon_{ikl}F_{kl},$$
$$F_{kl} = \partial_k A_l - \partial_l A_k - \frac{i}{\hbar}[A_k, A_l]. \tag{41}$$

Note that the term $\frac{1}{2}\epsilon_{ikl}[A_k, A_l] = (\boldsymbol{A} \times \boldsymbol{A})_i$ does not vanish in general, because the vector components of $\boldsymbol{A}$ do not necessarily commute. Therefore, the magnetic field $\boldsymbol{B}$ can be nonzero even if the vector potential $\boldsymbol{A}$ is uniform in space. This property is specific of non-Abelian dynamics and occurs only if $q \geq 2$, whereas for $q = 1$ we recover simply the Abelian dynamics discussed in the two preceding sections.

B. The multipod scheme

A generic way to obtain a degenerate subspace in atom-laser interaction is to realize the situation depicted in Fig. 6, where one single level labeled $|e\rangle$ is coupled to N levels labeled $|g_j\rangle$ ($j = 1, \ldots, N$), with complex Rabi frequencies κ_j (Juzeliūnas, Ruseckas, and Dalibard, 2010). We discuss at the end of this section how this scheme can be implemented in practice for $N = 3$ (tripod) and $N = 4$ (quadrupod). The atom-light coupling operator is

$$U = \sum_{j=1}^{N} \frac{\hbar\kappa_j(\boldsymbol{r})}{2}|e\rangle\langle g_j| + \text{H.c.}, \tag{42}$$

which can be conveniently rewritten as

$$U = \frac{\hbar\kappa(\boldsymbol{r})}{2}(|e\rangle\langle B(\boldsymbol{r})| + |B(\boldsymbol{r})\rangle\langle e|), \tag{43}$$

where $|B\rangle = \sum_{j=1}^{N} \kappa_j^*|g_j\rangle/\kappa$ is the bright (coupled) state generalizing Eq. (26) and κ is the total Rabi frequency, $\kappa^2 = \sum_{j=1}^{N} |\kappa_j|^2$.

The diagonalization of U is straightforward. First the coupling between $|B\rangle$ and $|e\rangle$ gives rise to the two eigenstates $|\pm\rangle = (|e\rangle \pm |B\rangle)/\sqrt{2}$ with energies $\pm\hbar\kappa/2$. Then the

remaining orthogonal subspace of dimension $N - 1$ corresponds to degenerate dark states that are all eigenstates of U with energy $\varepsilon = 0$. This provides the degenerate subspace $\mathcal{E}_q$ with $q = N - 1$ introduced in Sec. IV.A, which is required for the emergence of non-Abelian dynamics. In the following we denote $|D_n\rangle$ ($n = 1, \ldots, N - 1$) a normalized orthogonal basis of $\mathcal{E}_{N-1}$.

We briefly discuss how such a multipod scheme can be implemented in quantum optics for the two cases $N = 3$ and 4. The scheme of Fig. 6 for $N = 3$ is realized in a straightforward way by considering an atomic transition between a ground electronic state with angular momentum $J_g = 1$, and an excited electronic state with angular momentum $J_e = 0$. Such a transition occurs for alkali-metal species such as ^{23}Na or ^{87}Rb, as well as for helium atoms prepared in metastable electronic spin triplet states ($^3S_1 - {}^3P_0$ transition). The scheme $N = 4$ is a bit more subtle to achieve and we briefly outline the proposal detailed by Juzeliūnas, Ruseckas, and Dalibard (2010). The idea is to use the two hyperfine ground levels of an alkali-metal atom such as ^{87}Rb, with angular momenta equal to $F = 1$ and 2 (see Fig. 7). For the state $|e\rangle$ we choose one particular ground state $|e\rangle \equiv |F = 1, m = 0\rangle$. The four other states playing the role of the states $|g_j\rangle$ are the Zeeman sublevels $|F = 1, m_F = \pm 1\rangle$ and $|F = 2, m_F = \pm 1\rangle$. The couplings between $|e\rangle$ and the levels $|g_j\rangle$ are induced by resonant two-photon Raman transitions such as in Sec. III.D. The decoherence and heating due to photon scattering can be minimized in this scheme by choosing a large single-photon detuning (that is, of the order of the fine structure splitting Δ_{FS}), as explained in Sec. III.D.

C. Generating a magnetic monopole

One of the interesting properties of non-Abelian gauge potentials is the possibility to generate magnetic monopoles, as first pointed out by Moody, Shapere, and Wilczek (1986).
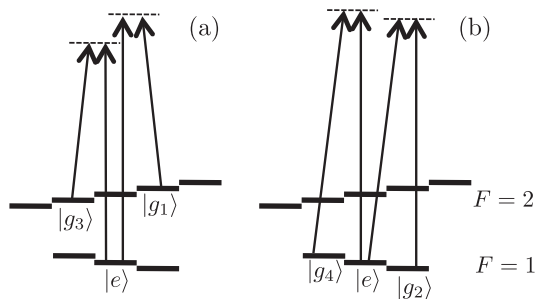

FIG. 7. Implementation of the multipod scheme for $N = 4$ for alkali-metal atoms with two hyperfine levels of angular momentum $F = 1$ and 2. The couplings involved in this scheme correspond to stimulated Raman transitions between hyperfine states of the ground levels. We choose $|e\rangle \equiv |F = 1, m_F = 0\rangle$. A small magnetic field lifts the degeneracy within the levels $F = 1$ and 2 and allows one to selectively address the various Raman transitions, using pairs of laser beams with properly chosen polarization and frequencies. (a) Two pairs of laser beams induce the transitions $|e\rangle \rightarrow |g_1\rangle \equiv |F = 2, m_F = 1\rangle$ and $|e\rangle \rightarrow |g_3\rangle \equiv |F = 2, m_F = -1\rangle$. (b) One additional pair of laser beams induce the transitions $|e\rangle \rightarrow |g_2\rangle \equiv |F = 1, m_F = 1\rangle$ and $|e\rangle \rightarrow |g_4\rangle \equiv |F = 1, m_F = -1\rangle$.

In this section we present a possible way to implement such a monopole using atom-light interaction. We concentrate on the physical aspects of the problem and we refer the interested reader to the original publication by Ruseckas *et al.* (2005) for technical details.

We consider here the tripod configuration obtained using $N = 3$ ground levels in the formalism of Sec. IV.B. It is convenient to parametrize the Rabi frequencies κ_j with angle and phase variables according to

$$\begin{aligned} \kappa_1 &= \kappa \sin\alpha \cos\beta e^{i\phi_1}, \\ \kappa_2 &= \kappa \sin\alpha \sin\beta e^{i\phi_2}, \\ \kappa_3 &= \kappa \cos\alpha e^{i\phi_3}, \end{aligned} \tag{44}$$

in which case we can choose the following expression for the dark states in the basis $\{|g_1\rangle, |g_2\rangle, |g_3\rangle\}$:

$$|D_1\rangle = \begin{pmatrix} \sin\beta e^{i\phi_{31}} \\ -\cos\beta e^{i\phi_{32}} \\ 0 \end{pmatrix},$$

$$|D_2\rangle = \begin{pmatrix} \cos\alpha \cos\beta e^{i\phi_{31}} \\ \cos\alpha \sin\beta e^{i\phi_{32}} \\ -\sin\alpha \end{pmatrix}, \tag{45}$$

with $\phi_{ij} = \phi_i - \phi_j$. The vector potential then reads

$$\begin{aligned} A_{11} &= \hbar(\cos^2\beta \nabla\phi_{23} + \sin^2\beta \nabla\phi_{13}), \\ A_{12} &= \hbar \cos\alpha[\tfrac{1}{2}\sin(2\beta)\nabla\phi_{12} - i\nabla\beta], \\ A_{22} &= \hbar\cos^2\alpha(\cos^2\beta \nabla\phi_{13} + \sin^2\beta \nabla\phi_{23}). \end{aligned} \tag{46}$$

To generate a magnetic monopole, we consider the laser setup formed with two of the laser beams propagating along the z axis, and the third one along the x axis. More precisely the first two beams are prepared in the Laguerre-Gauss modes with orbital angular momentum $\ell = \pm 1$, and the third beam is prepared in the first order Hermite-Gauss mode so that

$$\begin{aligned} \kappa_{1,2} &= \kappa_0 \frac{\rho}{R} e^{i(kz \mp \varphi)}, \\ \kappa_3 &= \kappa_0 \frac{z}{R} e^{ikx}. \end{aligned} \tag{47}$$

Here ρ is the distance from the z axis and φ the azimuthal angle around this axis. We suppose that the beam waists are large compared to the other physical scales of the problem and we therefore omit the Gaussian profiles in Eq. (47). The calculation of the vector potential using the formalism of Sec. IV.B gives

$$\begin{aligned} A = &-\frac{\hbar}{r\tan\vartheta} e_\varphi \hat{\sigma}_x + \frac{\hbar k}{2}(e_z - e_x)[(1 + \cos^2\vartheta)\hat{I} \\ &+ (1 - \cos^2\vartheta)\hat{\sigma}_z], \end{aligned}$$

where r, ϑ, and φ are the spherical coordinates, $\hat{\sigma}_j$ are the Pauli matrices, and $\hat{I}$ is the 2×2 unity matrix. The first term in the vector potential proportional to $\hat{\sigma}_x$ represents the field of a magnetic monopole of unit strength at the origin ($r = 0$):

$$B = \frac{\hbar}{r^2} e_r \hat{\sigma}_x + \cdots. \tag{48}$$

The dots indicate nonmonopole field contributions[1] proportional to the Pauli matrices and to the unity matrix. Note also that the total intensity of the laser fields (47) vanishes at the origin representing a singular point. Thus, one should apply an additional potential that will expel the atoms from this region, in order to avoid nonadiabatic transitions in the vicinity of $r = 0$.

This configuration was further analyzed by Pietilä and Möttönen (2009), who studied the behavior of an interacting Bose-Einstein condensate in this monopole configuration. They showed numerically that the existence of the monopole gives rise to a pseudospin texture with a topological charge that cancels the monopole charge.

D. Generating a spin-orbit coupling

Non-Abelian light-induced gauge potentials can be used for generating a spin-orbit coupling for cold atoms, simulating the one appearing for electrons in condensed matter. The electron's spin degree of freedom plays a key role in the emerging area of semiconductor spintronics (Zutic, Fabian, and Das Sarma, 2004; Fert, 2008; Grünberg, 2008). The first scheme for a semiconductor device is the spin field-effect Datta-Das transistor (DDT). It was proposed 20 years ago (Datta and Das, 1990) and implemented recently (Koo *et al.*, 2009). Atomic and polaritonic analogs of the electron spin transistor have also been suggested (Vaishnav *et al.*, 2008; Johne *et al.*, 2010). An important ingredient of the DDT is the spin-orbit coupling of the Rashba (Rashba, 1960; Winkler, 2003) or Dresselhaus (Dresselhaus, 1955; Schliemann, Egues, and Loss, 2003) types. This Rashba-Dresselhaus (RD) coupling scheme is described by a vector potential which can be made proportional to the spin-$\frac{1}{2}$ operator of a particle within a plane (Cserti and David, 2006).

We explain in this section how an effective spin-orbit coupling can be generated for atoms for the cases of an effective spin $s = 1/2$ and $s = 1$. We start with the general formalism of a N-pod level scheme in the case where the coupling lasers are plane waves of equal amplitude propagating in the x-y plane. More precisely we assume that the wave vectors k_j form a regular polygon

$$k_j = k(-e_x \cos\alpha_j + e_y \sin\alpha_j),$$
$$\alpha_j = 2\pi j/N. \tag{49}$$

We set $\kappa_j = \kappa^{(0)} e^{ik_j \cdot r}/\sqrt{N}$ and use the set of orthogonal normalized dark states

$$|D_n\rangle = \frac{1}{\sqrt{N}} \sum_{j=1}^{N} |g_j\rangle e^{i\alpha_j n - ik_j \cdot r},$$
$$n = 1, \dots, N-1. \tag{50}$$

Substituting $|D_n\rangle$ into Eqs. (39) and (40), one arrives at constant (yet non-Abelian) scalar and vector potentials

---

[1] A pure monopole would emerge if the Rabi frequencies κ_j could be taken proportional to the corresponding three Cartesian coordinates $\kappa_1 = Ax$, $\kappa_2 = Ay$, and $\kappa_3 = Az$. This is, however, not possible in practice, as this spatial dependence is not consistent with the Maxwell equations for the driving laser field.

$$W_{n,m} = \frac{\hbar^2 k^2}{4M} (\delta_{m,1}\delta_{n,1} + \delta_{m,N-1}\delta_{n,N-1}), \tag{51}$$

$$A_{n,m} = -\frac{\hbar k}{\sqrt{2}} \sum_{\pm} e_{\pm} \delta_{n,m\pm1}, \tag{52}$$

with $e_{\pm} = (e_x \pm ie_y)/\sqrt{2}$. For a constant external potential V, a basis of stationary solutions of the Schrödinger equation (38) are the plane waves $\tilde{\Psi}_K(r, t) = \Phi_K e^{i(K \cdot r - \Omega_K t)}$ with the amplitude Φ_K obeying the eigenvalue equation $H_K \Phi_K = \hbar \omega_K \Phi_K$, where H_K is the K-dependent $(N-1) \times (N-1)$ matrix:

$$H_K = \frac{(\hbar K \hat{1} - A)^2}{2M} + W + V\hat{1}. \tag{53}$$

In the tripod setup ($N = 3$) the wave vectors k_j form an equilateral triangle and W, A, and H_K are 2×2 matrices. The scalar potential is proportional to the unit matrix $W = (\hbar^2 k^2/4M)\hat{1}$, whereas the vector potential $A = -k\hat{S}_\perp$ is proportional to the spin-$\frac{1}{2}$ operator $\hat{S}_\perp = \hat{S}_x e_x + \hat{S}_y e_y$ in the x-y plane ($\hat{S} = \hbar\hat{\sigma}/2$, where the $\hat{\sigma}$ are the Pauli matrices). This provides a spin-orbit coupling of the RD type, characterized by two dispersion branches $\Omega_K^{\pm} = \hbar(K \pm k/2)^2/2M$ for $V = -\hbar^2 k^2/(4M)$. A number of other arrangements of laser beams have been considered to produce the same RD spin-orbit coupling (Jacob *et al.*, 2007; Stanescu, Zhang, and Galitski, 2007; Juzeliūnas, Ruseckas, Lindberg *et al.*, 2008; Vaishnav and Clark, 2008; Larson and Sjöqvist, 2009; Zhang, Gong, and Oh, 2010).

In the tetrapod setup ($N = 4$) the choice of Eq. (49) corresponds to two orthogonal pairs of counterpropagating laser fields. The vector potential $A = -k\hat{J}_\perp/\sqrt{2}$ is proportional to the projection of a spin 1 operator in the x-y plane $\hat{J}_\perp = \hat{J}_x e_x + \hat{J}_y e_y$, whereas the scalar potential is proportional to the squared z component of the spin operator, $W = \hat{J}_z^2 k^2/(4M)$. The eigenfrequencies are now

$$\hbar\Omega_K^{\beta} = \frac{\hbar^2}{2M}(K^2 + \sqrt{2}Kk\beta + k^2) + V,$$
$$\beta = 0, \pm 1, \tag{54}$$

with $K = |K|$. For $\beta = \pm 1$ the dispersion curves are analogous to those of the spin-$\frac{1}{2}$ RD model. The additional dispersion curve with $\beta = 0$ corresponds to a parabola centered at $K = 0$.

A spectacular consequence of spin-orbit RD coupling is the Zitterbewegung, a phenonenon which was analyzed for cold atoms (Merkl *et al.*, 2008; Vaishnav and Clark, 2008; Song and Foreman, 2009; Larson, Martikainen, and Collin, 2010), electrons in solids (Cserti and David, 2006; Schliemann, Loss, and Westervelt, 2006; Rusin and Zawadzki, 2009), and trapped ions (Lamata *et al.*, 2007; Rusin and Zawadzki, 2010). It was recently observed for the latter systems (Gerritsma *et al.*, 2010). Another manifestation of the RD coupling is the negative refraction and reflection that occurs when a matter wave is incident on a potential step. This problem was investigated for spin-$\frac{1}{2}$ atoms (Juzeliūnas, Ruseckas, Jacob *et al.*, 2008) and electrons (Teodorescu and Winkler, 2009; Dargys, 2010). For small incident wave numbers $K \ll k$, the transmission probability is close to unity

for normal incidence. This nearly complete transmission is a manifestation of the Klein paradox appearing also for electron tunneling in graphene (Katsnelson, Novoselov, and Geim, 2006; Castro Neto *et al.*, 2009). The transmission probability decreases when the angle of incidence increases, and the transmitted matter wave experiences negative refraction, again similar to electrons in graphene (Cheianov, Fal'ko, and Altshuler, 2007). Particles with a spin larger than $\frac{1}{2}$ have additional internal degrees of freedom, which modifies the continuity conditions at the potential step. For the negative refraction phenomenon at non-normal incidence, Juzeliūnas, Ruseckas, and Dalibard (2010) showed that the amplitude of the refracted beam is significantly increased in comparison with the spin-$\frac{1}{2}$ case.

Spin-orbit coupling with its multicomponent dispersion curves also offers interesting scenarios in the presence of collisional interactions (Stanescu, Zhang, and Galitski, 2007; Stanescu, Anderson, and Galitski, 2008; Wang *et al.*, 2010; Yip, 2011; Zhou and Wu, 2011). In two dimensions with a symmetric RD gauge potential of the form $\hbar k(\sigma_x \boldsymbol{e}_x + \sigma_y \boldsymbol{e}_y)$, the dispersion curve has a minimum at a constant nonzero radius in momentum space. This corresponds to a massive degeneracy of the single-particle ground level, since all plane waves with momentum $\boldsymbol{K}$ such that $|\boldsymbol{K}| = k$ are possible ground states. For a Bose gas, this precludes in principle the formation of a condensate, and atomic interactions will lead to the formation of a strongly correlated ground state. However, in the presence of an asymmetry in the RD coupling, the massive degeneracy is lifted and the minimum of the dispersion occurs for two opposite values of the atomic momenta (Stanescu, Zhang, and Galitski, 2007; Stanescu, Anderson, and Galitski, 2008). Weakly interacting bosons with such RD coupling will then behave essentially as a two-component system at low temperature.

We conclude by signaling a possible drawback of the tripod scheme: The two dark state states forming the effective spin-$\frac{1}{2}$ system are not the lowest single-particle energy states, hence collisional deexcitation can transfer the atoms out of the dark state manifold down to the ground dressed state. To overcome this difficulty, a scheme involving N ground or metastable internal states cyclically coupled by laser fields was recently proposed (Campbell, Juzeliūnas, and Spielman, 2011). By properly setting the direction and phases of the laser fields, a pair of degenerate pseudospin states with lowest energy emerge. The states are subjected to the RD coupling and are immune to the collisional decay.

E. Non-Abelian Aharonov-Bohm effect

The spin-orbit coupling presented in the preceding section can also be the source of quasirelativistic dynamics, where the atomic center-of-mass motion is governed by an effective Dirac equation in the limit of small momenta and strong gauge potentials. The quasirelativistic dynamics of the atomic center of mass is a remarkable effect which connects phenomena from high energy physics, graphene, and photonic crystals with atomic physics and quantum optics. It relies on the two- or three-component nature of the effective atomic internal structure, but it is not explicitly linked to the non-Abelian nature of the coupling.

To observe a non-Abelian effect one should study spin dynamics. In our case it will be a pseudospin, i.e., an effective multicomponent system created by the interaction between incident laser beams and the atoms. Previously we have shown that the gauge potential affecting the pseudospin can be, for instance, proportional to the Pauli spin matrices in the x and y directions such that the matrices corresponding to the two directions do not commute. This is indeed also the requirement for having a non-Abelian system. A simple illustration of a non-Abelian situation is the so-called non-Abelian Aharonov-Bohm experiment (Jacob *et al.*, 2007). Here we envisage a particle with an internal structure, the pseudospin, which is allowed to move along two different paths from A to B along straight lines in the x and y directions. Suppose the path consists of two equidistant trips of length L along the x and y directions. The question is, if we start at A, with a given orientation of the pseudospin, what is the spin at the final point B? If the spin is subject to a non-Abelian field, the result will depend on which path the particle took. This is easily seen by neglecting any external dynamics and considering only the effects from the gauge potential, which is of the form $\boldsymbol{A} = A_x \boldsymbol{e}_x + A_y \boldsymbol{e}_y$. The final state based on the path going first along the x direction and then the y direction will be given by $\exp[iA_y L]\exp[iA_x L]\tilde{\Psi}_{\mathrm{in}}$, where $\tilde{\Psi}_{\mathrm{in}}$ is the initial pseudospin. If we take the path along the y direction first and then in the x direction, we have the final state $\exp[iA_x L]\exp[iA_y L]\Psi_{\mathrm{in}}$. These two states are not necessarily the same, because A_x and A_y do not commute if the system is non-Abelian. For instance, when $A_x \propto \hat{\sigma}_y$ and $A_y \propto \hat{\sigma}_x$, these operations are equivalent to spin rotations around x and y, which do not yield the same final state in general. Interestingly this situation is similar to the scattering of protons onto a non-Abelian flux line where the protons are anticipated to be converted into neutrons (Horváthy, 1986).

V. GAUGE POTENTIALS IN OPTICAL LATTICES

Optical lattices have recently emerged as a major tool for the field of quantum gases [see Lewenstein *et al.* (2007) and Bloch, Dalibard, and Zwerger (2008) for recent reviews]. They correspond to a periodic array of trapping sites connected to each other by quantum tunneling. Such a potential landscape is created using the interference pattern of several off-resonant lasers. In addition to the obvious analogy with the effective periodic potential exerted by the ionic matrix on electrons in a real solid, optical lattices allow one to bring quantum gases into the strongly correlated regime, where interactions dominate the behavior of the system. The entrance in the correlated regime is obtained by increasing the lattice depth and it follows from two effects, the increase of the on-site interaction energy due to the stronger confinement of the atoms near the lattice sites, and the reduction of the tunneling probability from site to site which decreases the kinetic energy.

In this section we first review some basic elements on the band structure in a periodic potential (Sec. V.A) and the effects of a magnetic field on the single-particle spectrum (Sec. V.B). We then discuss the concept of *laser-assisted tunneling*, which allows one to control the phase of the tunneling matrix elements and realize artificial gauge potentials

(Secs, V.C and V.D). Recently another class of lattices with orbital magnetism, the so-called *flux lattices*, has been proposed by Cooper (2011). We briefly relate this proposal as well as those based on laser-assisted tunneling to the dressed state approach discussed in Sec. V.E. Finally we give a short account on the possibility to generate non-Abelian fields in lattices in Sec. V.F.

We briefly mention some alternative methods that do not use laser coupling to realize effective magnetic fields for cold atoms in optical lattices. One is simply to rotate the lattice, which was realized experimentally by Tung, Schweikhard, and Cornell (2006) and Williams, Al-Assam, and Foot (2010) for lattices with large lattice spacing, i.e., outside the Hubbard regime. Another method relies on a temporal modulation of the lattice potential with $x - y$ (Sørensen, Demler, and Lukin, 2005) or $x^2 - y^2$ (Lim, Smith, and Hemmerich, 2008) symmetries [see also Kolovsky (2011)]. One can also control the sign of the tunneling matrix element by modulating the lattice potential (Eckardt, Weiss, and Holthaus, 2005; Lignier *et al.*, 2007), which can provide artificial magnetism for some specific lattice geometries. Finally one can obtain the desired gauge potential through interactions with a bath of atoms (Klein and Jaksch, 2009).

A. Reminder on band structure

Consider a particle moving in the two-dimensional square lattice potential with period d and depth V_0:

$$V_{\mathrm{lat}}(x, y) = V_0[\sin^2(\pi x/d) + \sin^2(\pi y/d)]. \quad (55)$$

The energy eigenstates are the Bloch waves $\psi_{\eta,q}(r) = e^{iq \cdot r} u_{\eta,q}(r)$, where $\eta = 0, 1, \ldots$ denotes the band index and the quasimomentum q takes values in the first Brillouin zone (BZ) $[-\pi/d, \pi/d[\times[-\pi/d, \pi/d[$ [see, for example, Ashcroft and Mermin (1976)]. The function $u_{\eta,q}$ is a periodic function of r, with period d along both directions of space. The energies $\epsilon_\eta(q)$ associated with the Bloch waves form bands when q is varied inside the first Brillouin zone.

We assumed in the following that the lattice is in the tight-binding (TB) regime, where the energy width of each band is much smaller than the gaps between two consecutive bands. More specifically, we consider particles confined to the lowest Bloch band $\eta = 0$ as it is usually the target regime for experiments on correlated quantum gases, and we subsequently drop the band index. In this limit, it is useful to transform to the orthogonal basis of Wannier functions

$$w_{n,m}(r) = \mathcal{N} \int_{\mathrm{BZ}} e^{-iq \cdot r_{n,m}} \psi_q(r) d^2 q, \quad (56)$$

where $\mathcal{N}$ is a normalization factor and $r_{n,m} = d(n e_x + m e_y)$, with n, m being integers. In the TB regime, the Wannier function $w_{n,m}$ is localized near the lattice site at position $r_{n,m}$ and the initial Hamiltonian $P^2/(2M) + V_{\mathrm{lat}}$ can be replaced by

$$H_{\mathrm{TB}} = -J \sum_{\mathrm{n.n.}} \hat{a}_{n,m}^\dagger \hat{a}_{n',m'}, \quad (57)$$

where $\hat{a}_{n,m}$ is an annihilation operator for a particle in the state $w_{n,m}$. The sum runs over nearest neighbors (n.n.) only, and J is the tunneling energy characterizing the hopping between neighboring sites. Hopping to more distant sites is neglected

in this approximation. The single-particle dispersion is in the TB approximation $\epsilon(q) = -2J[\cos(q_x d) + \cos(q_y d)]$, corresponding to an energy width of $8J$ for the band.

B. Harper equation and Hofstadter butterfly

Suppose now that the square lattice considered above is placed in a uniform magnetic field $B = Be_z$, associated with the vector potential $A = (-By, 0, 0)$ (Landau gauge). For a particle carrying a charge e, the Hamiltonian (57) can be written

$$H = -J \sum_{n,m,\pm} e^{\pm i\phi_{n,m}} \hat{a}_{n\pm 1,m}^\dagger \hat{a}_{n,m} - J \sum_{n,m,\pm} \hat{a}_{n,m\pm 1}^\dagger \hat{a}_{n,m}, \quad (58)$$

with

$$\phi_{n,m} = \frac{e}{\hbar} \int_{r_{n,m}}^{r_{n+1,m}} A \cdot ds, \quad (59)$$

where the integral is taken along a straight line joining neighboring sites. The appearance of the phase factors $e^{\pm i\phi_{n,m}}$ in Eq. (58) can be understood in terms of the Aharonov-Bohm phase accumulated along a straight line joining two adjacent sites of the lattice. With the choice of the Landau gauge, these phase factors are

$$r_{n,m} \to r_{n+1,m} : \phi_{n,m} = 2\pi\alpha m, \quad (60)$$

where $\alpha = \Phi/\Phi_0$, $\Phi = Bd^2$ is the magnetic flux through a unit cell, and $\Phi_0 = h/e$ is the flux quantum. A different gauge choice leads to different phase factors $\phi_{n,m}$, but the phase accumulated on a closed circuit around an elementary cell

$$\gamma = \sum_\square \phi_{n,m} = eBd^2/\hbar = 2\pi\alpha \quad (61)$$

is gauge invariant (the symbol $\square$ indicates that the sum runs over an elementary cell of the lattice).

The reduction of the full Schrödinger equation to Eq. (58) involves another approximation, the so-called Peierls's substitution [see Luttinger (1951) for a discussion of this approximation in the TB limit]. It is valid if the Landau energy $\hbar\omega_c$, where $\omega_c = B/M$ is the cyclotron frequency, remains much smaller than the energy gap between the bands $n = 0$ and 1. Outside of the TB regime, its validity has to be carefully examined (Nenciu, 1991). In the context of our Colloquium, these considerations are not relevant as we discuss methods to simulate the Hamiltonian (58) directly.

The single-particle eigenstates of the Hamiltonian (58) can be searched in the form $\sum_{m,n} C_m e^{iq_x nd} \hat{a}_{n,m}^\dagger |\mathrm{vac}\rangle$. The corresponding eigenvalue equation for the coefficients C_m is known as the Harper equation (Harper, 1955). Its solutions have been extensively studied in connection with the quantum Hall effect (Thouless *et al.*, 1982; Kohmoto, 1989). The energy spectrum, represented in Fig. 8, is known as the *Hofstadter butterfly* (Hofstadter, 1976), and it exhibits a remarkable self-similarity. This spectrum has a much more complex structure than its counterpart for a continuous system, the latter being composed of uniformly spaced, infinitely degenerate Landau levels. This structure can be qualitatively
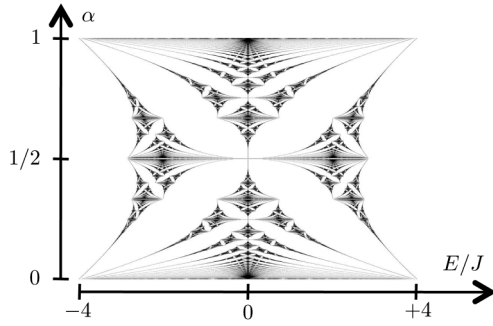
FIG. 8. Hofstadter butterfly: single-particle spectrum of the Hamiltonian of Eq. (58) in units of the tunneling amplitude J, for $\alpha = \phi/\phi_0$ varying between 0 and 1.

understood on a relatively simple ground. For a rational value of α, that is $\alpha = p/q$ with p, q integers, the Hamiltonian is still periodic but with a larger period qd along the y axis. One can then divide the system into "macrocells" of size qd and look for new eigenstates [the so-called *magnetic Bloch functions* (Blount, 1962)] appropriate for the "macrolattice." Because the macrocell contains q original lattice sites, the fundamental band splits into q subbands generally separated by small energy gaps (with some exceptions, such as the case $\alpha = 1/2$, where the two bands touch at the edges of the reduced Brillouin zone). The Landau levels structure is recovered in the weak flux limit where $\alpha = p/q \ll 1$. We note finally the special case of $\alpha = 1/2$, corresponding to a real tunneling matrix element alternating in sign from one column to the next. In this case, the excitation spectrum features two "Dirac points" for $(k_x, k_y) = (\pm \pi/d_x, \pi/2d_y)$ around which the dispersion relation is linear (Hatsugai and Kohmoto, 1990; Lim, Smith, and Hemmerich, 2008; Hou, Yang, and Liu, 2009). The behavior of an ultracold Fermi gas in such a situation is expected to be similar to that observed in graphene (Castro Neto *et al.*, 2009).

C. Simulating a magnetic flux through each lattice cell

We now discuss how the Hamiltonian (58) can be realized for cold atoms in an optical lattice. We proceed in two steps. First we introduce the notion of laser-assisted tunneling and show how it can be used to obtain a nonzero flux through each lattice cell. However, laser-assisted tunneling in its simplest version provides a flux that alternates in sign between neighboring cells and thus does not simulate a uniform magnetic field. In the second step (Sec. V.D), we show how one can rectify this magnetic flux and reach the Hamiltonian (58).

The notion of laser-assisted tunneling was introduced in this context by Ruostekoski, Dunne, and Javanainen (2002) and Jaksch and Zoller (2003). The first ingredient is to design a *state-dependent lattice*. Consider atoms with two internal states g and e, trapped in spatially separated sublattices (see Fig. 9). We focus on the situation where each sublattice has rectangular symmetry with lattice spacings d_x and d_y. The e sublattice is deduced from the g sublattice by a translation $d_x/2$ along the x axis. We label

$$\mathbf{r}_{2n,m}^{(g)} = n d_x \mathbf{e}_x + m d_y \mathbf{e}_y, \tag{62}$$

$$\mathbf{r}_{2n+1,m}^{(e)} = (n + 1/2) d_x \mathbf{e}_x + m d_y \mathbf{e}_y, \tag{63}$$
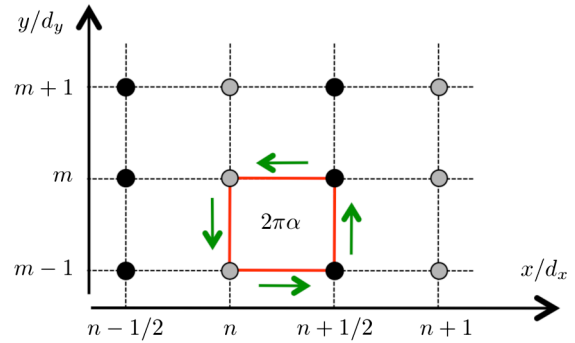

FIG. 9 (color online). Sketch of the state-dependent 2D lattice potential. Gray (black) dots mark lattice sites for atoms in the ground g (excited e) state. We highlight a trajectory around an elementary cell of the coupled lattice in which the particle acquires the Aharonov-Bohm phase $2\pi\alpha$. The $g \rightarrow g$ and $e \rightarrow e$ transitions occur due to standard tunneling. The $g \rightarrow e$ and $e \rightarrow g$ transitions correspond to resonant laser-assisted tunneling. In a $g \rightarrow e$ transition the atom absorbs a photon and jumps from a state localized around $x = n d_x$ to a state localized around $x = (n \pm 1/2) d_x$ (and vice versa for a $e \rightarrow g$ transition).

the positions of the trapping sites on each sublattice, with the corresponding Wannier functions $w_{2n,m}^{(g)}$ and $w_{2n+1,m}^{(e)}$. Tunneling energies along x and y within a given sublattice (g or e) are denoted by J_x and J_y, respectively.

In practice, there are two options to generate such a state-dependent lattice. The first one, suitable for alkali atoms, selects g and e as two Zeeman or hyperfine states in the electronic ground state manifold (electronically excited states are too short lived for this application). In this case, the leading term in the optical lattice potential is the sum of scalar and vector terms, the latter behaving as an effective magnetic field (Cohen-Tannoudji and Dupont-Roc, 1972). The states g and e are chosen such that they have opposite magnetic moments, and the detuning from resonance of the light beams forming the x lattice is adjusted so that the polarizabilities of g and e are opposite (Mandel *et al.*, 2003). This provides the desired state-dependent lattice potential along the x axis. Note, however, that the required detuning lies relatively close to the resonance lines, so that heating due to photon scattering can cause serious practical problems.

The second option is to use atomic species already considered in Sec. II.B with a long-lived excited state (Yi *et al.*, 2008; Gerbier and Dalibard, 2010). Practical examples are alkaline-earth or ytterbium atoms, where the $^3P_0$ internal state has a typical lifetime over 10 s. One then chooses the electronic (spin singlet) ground state for g and the $^3P_0$ excited state for e. For such atoms, both states couple to different electronic states, and it is possible to find a *magic* wavelength (used for the y lattice) such that the polarizabilites are identical for both states, and an *antimagic* wavelength (used for the x lattice) such that they are opposite. Both are far detuned from any resonance, so that heating by spontaneous emission is not an issue in this case.

In a state-dependent lattice, tunneling from a given site on the g sublattice to a neighboring one on the e sublattice can be driven by a resonant light field that couples g and e. We assume this coupling laser is a plane running wave with wave

vector $\boldsymbol{k}$. The corresponding complex tunneling matrix element is

$$g, \boldsymbol{r}_{2n,m}^{(g)} \rightarrow e, \boldsymbol{r}_{2n\pm1,m}^{(e)}: J_{\mathrm{eff}} = \hbar\kappa^{(0)}\mathcal{O}e^{i\boldsymbol{k}\cdot\boldsymbol{r}_{2n,m}^{(g)}}, \qquad (64)$$

where $\kappa^{(0)}$ characterizes the strength of the atom-laser coupling and the dimensionless number,

$$\mathcal{O} = \int [w_{2n+1,m}^{(e)}(\boldsymbol{r})]^* w_{2n,m}^{(g)}(\boldsymbol{r}) e^{i\boldsymbol{k}\cdot\boldsymbol{r}} d^2r, \qquad (65)$$

is the overlap integral between neighboring Wannier functions (Jaksch and Zoller, 2003) (note that $w_{2n,m}^{(g)}$ and $w_{2n+1,m}^{(e)}$ are not orthogonal since they belong to different sublattices). Equation (64) displays the essential phase factor that allows one to reproduce the Aharonov-Bohm phase (59). By choosing a laser propagating in the y-z plane, and under the assumption that state-independent tunneling along x is negligible ($J_x \ll |J_{\mathrm{eff}}|$), one obtains

$$\begin{aligned} H = &-|J_{\mathrm{eff}}| \sum_{n,m,\pm} e^{i\phi_m} \hat{b}_{2n\pm1,m}^\dagger \hat{a}_{2n,m} + \mathrm{H.c.} \\ &- J_y \sum_{n,m,\pm} \hat{a}_{2n,m\pm1}^\dagger \hat{a}_{2n,m} + \hat{b}_{2n+1,m\pm1}^\dagger \hat{b}_{2n+1,m}, \end{aligned} \qquad (66)$$

where $\hat{a}_{2n,m}^\dagger$ ($\hat{b}_{2n+1,m}^\dagger$) creates an atom in the internal state g (e) in the state $w_{2n,m}^{(g)}$ ($w_{2n+1,m}^{(e)}$). Here $e^{i\phi_m}$ is the complex phase of J_{eff}, characterizing the phase acquired by an atom when it tunnels from a site of the sublattice g to a site of the sublattice e:

$$g, \boldsymbol{r}_{2n,m}^{(g)} \rightarrow e, \boldsymbol{r}_{2n\pm1,m}^{(e)}: \phi_{2n,m} = 2\pi\alpha m, \qquad (67)$$

where $\alpha = k_y d_y/(2\pi)$ can be adjusted between 0 and 1 by changing the angle of the wave vector $\boldsymbol{k}$ of the coupling laser with the y axis.

Although the Hamiltonian (66) contains complex hopping amplitudes, it does not yet coincide with the Hamiltonian (58) that we want to simulate. In the initial Hamiltonian, the phase picked up across each x link has the same sign for a given link direction in real space: $2\pi\alpha m$ in the $+x$ direction (and thus $-2\pi\alpha m$ in the $-x$ direction since the Hamiltonian is Hermitian). Here the phase is tied to the direction in internal space: $2\pi\alpha m$ for transitions to g to e, irrespective of the fact that they occur in the $+x$ or $-x$ directions.

In total, we achieve with Eq. (66) a situation where the flux through a cell changes sign from one cell to the next one along the x axis. We anticipated this difficulty in Sec. II.E, where we noted that realizing artificial gauge potentials with variations on the scale of the optical wavelength λ_L would naturally result in an oscillating (or *staggered*) effective magnetic field. Although this configuration can lead to interesting situations (Wang and Gong, 2006; Hou, Yang, and Liu, 2009; Möller and Cooper, 2010), it does not realize our goal of producing a uniform magnetic field, except for the specific case $\alpha = 1/2$, since phase changes of $\pm\pi$ are equivalent.

D. Rectification of the magnetic field in the lattice

The need for rectification of the magnetic field that we found in the preceding section can be formulated on more general grounds. We are looking for an effective Hamiltonian that must break time-reversal symmetry. For our two-level system, the time-reversal operator is $\mathcal{T} = \mathcal{K}_s\mathcal{K}_c$ (Messiah, 1961a), where $\mathcal{K}_s = e^{i\pi\hat{\sigma}_y/2} = i\hat{\sigma}_y$ is such that $\mathcal{K}_s|g\rangle = |e\rangle$, $\mathcal{K}_s|e\rangle = -|g\rangle$, and $\mathcal{K}_c$ is the conjugation operator. Now, the action of $\mathcal{T}$ on the configuration studied in the previous section results in the same configuration, except for a mere translation by an amount $d_x/2$ along the x axis. Hence, in order to produce a uniform magnetic field, one must add another ingredient that is not symmetric under the "sublattice translation" operation.

Jaksch and Zoller (2003) proposed to realize this by adding a linear potential gradient along x, $V_{\mathrm{grad}}(n) = \zeta n$, so that the laser frequency for the $(g; 2n, m) \rightarrow (e; 2n + 1, m)$ transition becomes shifted by $+\zeta$ while that for the $(g; 2n + 2, m) \rightarrow (e; 2n + 1, m)$ transition is shifted by $-\zeta$. By choosing $\zeta \gg |J_{\mathrm{eff}}|$, the two transition frequencies become nondegenerate and must be addressed by two different lasers. One then chooses the laser resonant with $(g; 2n, m) \rightarrow (e; 2n + 1, m)$ to propagate along $+\boldsymbol{e}_y$, and the laser resonant with $(e; 2n + 1, m) \rightarrow (g; 2n + 2, m)$ to propagate along $-\boldsymbol{e}_y$. According to Eq. (64), the sign of the phase factor changes on every second column, which results in a rectification of the staggered field to a uniform one (provided off-resonant terms are negligible compared to resonant ones). Practically, such a potential gradient can be implemented by a real electric field affecting g and e equally, or by the ac Stark shift exerted by an off-resonant laser. The large electric fields or optical powers involved, combined with the fact that the tilting potential must be linear over the whole cloud to ensure a uniform transition frequency, make this option challenging from an experimental point of view.

A possibly more practical configuration is based on a superlattice potential with period $2d_x$ along x on the top of the main lattice, which can perform the same role as the potential gradient mentioned previously (Gerbier and Dalibard, 2010). One needs three (instead of two) different coupling laser frequencies in this case, but this is not a significant increase in difficulty since the frequency differences are in the tens of kHz range, and can thus be easily generated using frequency modulators. Another proposal by Mueller (2004) realized the same goal by using three internal states in three different sublattices. In that case, the distinction between neighboring transitions is automatic, and there is no need for an additional external potential. Unfortunately this trapping configuration seems difficult to implement in practice for the commonly used atomic species.

E. Connection with dressed state approach

It is interesting to establish a link between the optical lattice case and the schemes discussed in Secs. II and III, where we assumed that the atoms were following adiabatically one internal dressed state, defined as one of the local eigenstates of the atom-laser coupling matrix. We first discuss the case of lattices with laser-assisted tunneling that we considered in the first part of this section. We then briefly present the concept of flux lattices recently introduced by Cooper (2011).

Lattices with laser-assisted tunneling.—The dressed states can of course also be defined in the lattice case. For

simplicity we take a uniform Rabi frequency $\kappa^{(0)}$ for the coupling laser and a spatially varying detuning $\Delta(\boldsymbol{r}) = \Delta_0 + [V_e(\boldsymbol{r}) - V_g(\boldsymbol{r})]/\hbar$, where V_g and V_e denote the potential energies for the g and e sublattices, respectively. We denote V_0 as the characteristic amplitude of oscillation of V_e and V_g, and we assume that $\hbar\kappa^{(0)} \ll V_0$ to ensure that the coupling laser does not lead to a strong deformation of the state-dependent lattice potential. As explained in Sec. II.C, this corresponds to a situation such that the mixing angle θ varies rapidly around the points where the resonance condition $\Delta(\boldsymbol{r}) = 0$ occurs. We use as a typical value $|\boldsymbol{\nabla}\Delta| \approx kV_0/\hbar$, where k is a typical optical wave number. From the discussion of Sec. II.C, we obtain the validity condition for the adiabatic approximation $\kappa^{(0)} \gg \sqrt{V_0 E_{\mathrm{R}}}/\hbar$. In the TB limit the right-hand side is approximately the frequency gap ω_{gap} between the ground ($\eta = 0$) and the first excited ($\eta = 1$) band. With the adiabaticity condition now written as $\kappa^{(0)} \gg \omega_{\mathrm{gap}}$, we immediately conclude that the adiabatic following of a given dressed state is intrinsically incompatible with the single-band model used in this section. In other words the laser-assisted tunneling scheme considered in this section is a ''diabatic process'' (Smith, 1969) with respect to the dressed state basis, and it is therefore qualitatively different from the adiabatic scheme considered in Secs. II and III to generate artificial gauge fields in a bulk system.

Flux lattices.—(Cooper, 2011) A flux lattice is based on a purely periodic 2D pattern of interfering laser fields. Atoms are modeled as two-level systems as in Sec. II, with a coupling matrix U in Eq. (2) whose coefficients Ω, θ, and ϕ are periodic functions of x and y. In the adiabatic limit studied in Sec. II, the vector potential $\boldsymbol{A}$ calculated from Eq. (7) is also a periodic function of x and y. One could then think that the flux of the magnetic field across a unit cell of the lattice, which is equal to the circulation of $\boldsymbol{A}$ on the contour of the cell, is always zero. However, this does not hold if the laser field is chosen such that $\boldsymbol{A}$ has singularities inside the cell. Such singularities occur at locations where $\sin\theta = 0$, so that ϕ is ill defined. Contrary to $\boldsymbol{A}$, the magnetic field $\boldsymbol{B}$ in these points, calculated from Eq. (8), is nonsingular. Cooper (2011) showed that configurations exist where B_z keeps a constant sign over the cell,[2] with a magnitude $\sim \hbar k^2$. In particular, the Chern number of the lowest allowed energy band (Thouless *et al.*, 1982) can be nonzero. This scheme, which is actually still valid outside the adiabatic limit (Cooper and Dalibard, 2011), thus constitutes an attractive alternative to the ones based on laser-assisted tunneling.

F. Non-Abelian gauge fields in a lattice

Optical lattices are also well suited for the generation of artificial non-Abelian magnetic fields, as first proposed by

---

[2]More precisely, the total field consists of a regular background component with nonzero average, plus a periodic array of gauge-dependent Dirac strings, located in points where $\cos\theta = -1$ for the gauge choice of Eq. (3), and carrying a flux of opposite sign as compared to the background. The regular and singular components together give a zero net flux over an elementary cell, as expected for a periodic Hamiltonian. However the Dirac strings are nonmeasurable and only the background component has an observable effect.

Osterloh *et al.* (2005), and we conclude this section by a brief description of a possible implementation. As in Sec. IV, the basic idea to generate non-Abelian potentials is to use several internal atomic levels that are coupled by various laser beams. Here we consider an atomic species with $2N$ quasidegenerate sublevels, trapped either in sublattice g (sublevels g_i, $i = 1, \ldots, N$) or in sublattice e (sublevels e_j, $j = 1, \ldots, N$). Instead of a simple phase, laser-induced couplings must induce a rotation in internal space, generated by a $N \times N$ matrix $\boldsymbol{M}$ with noncommuting components M_x, M_y, and M_z. Consider for instance a species with spin $\frac{1}{2}$ in both the ground and excited manifolds (the spin $\frac{1}{2}$ plays the role of a fictitious ''color'' charge here), which moves in an optical lattice that is now state dependent along both x and y. Laser-induced tunneling is used along both axes, with the additional possibility of changing the spin index $m_z = \pm 1/2$. For instance, the lasers inducing tunneling along y can be chosen to flip the spin ($m_z \rightarrow m_z' = -m_z$), so that $M_y \propto \alpha \hat{\sigma}_x + \beta \hat{\sigma}_y$, where α and β are numerical coefficients depending on the laser phases. The lasers inducing tunneling along x are then chosen to preserve the spin ($m_z \rightarrow m_z' = m_z$), so that $M_x \propto \gamma \hat{1} + \delta \hat{\sigma}_z$. Provided that $\delta \neq 0$, i.e., the x lasers apply a different phase conditionally on the internal color, this realizes a non-Abelian potential. The physical effects that one expects from this non-Abelian setting are similar to those discussed in Sec. IV, in particular, the emergence of a Rashba-like spin-orbit coupling (Dudarev *et al.*, 2004; Osterloh *et al.*, 2005; Goldman, 2007; Satija *et al.*, 2008; Goldman, 2009; Goldman *et al.*, 2009a, 2009b).

VI. OUTLOOK

In this Colloquium we presented the physical principles that lead to the generation of artificial gauge potentials on neutral atoms, using their coupling to laser fields. We considered the cases of bulk systems and discrete lattices, and we showed that both Abelian and non-Abelian gauge potentials are accessible, provided one chooses a suitable atomic level structure and proper incident light fields. We also explored several physical consequences of these gauge fields, such as the nucleation of quantized vortices in a superfluid, the generation of a spin-orbit coupling via a non-Abelian gauge field, or the possibility to address the strong magnetic field limit in a 2D lattice with the corresponding Hofstadter butterfly energy spectrum. The variety of items in this (incomplete) list shows the richness of the situations that can be realized.

These artificial fields also constitute novel tools for characterizing the properties of an assembly of atoms. Cooper and Hadzibabic (2010) suggested using a small artificial magnetic field to probe the superfluidity of a gas. The field is generated with a laser scheme close to the one of Sec. III.B, and it is used to simulate a *rotating bucket* experiment and measure the reduced moment of inertia of a fluid when it acquires a superfluid component. In presence of the artificial field the normal component will stay at rest in the laboratory frame, whereas the superfluid component will rotate. A key feature of this proposal is that one can use spectroscopic methods to access the respective populations of the superfluid and normal states, by measuring the populations of the various ground states g_j involved in the process.

In order to keep this Colloquium within reasonable limits, we intentionally restricted our analysis to single-particle or mean-field physics. However, it is clear that these gauge fields can lead to interesting phenomena when combined with the richness of strongly correlated states that emerge in many-body physics. For the Abelian case in the continuum limit, the situation is similar to the case of rotating gases, and paths to quantum Hall physics that have been identified for Bose and Fermi gases remain of order [for a review, see Cooper (2008)]. In the context of the Bose-Hubbard model in the presence of a uniform magnetic field, Möller and Cooper (2009) recently proposed an approach based on the composite fermion theory to establish the existence of strongly corre-lated phases that have no equivalent in the continuum limit [see also Polak and Kopeć (2009)]. Another line of research with optical lattices deals with the combination of artificial gauge fields and nearest-neighbor interactions, as recently explored by Ruostekoski (2009).

To end on a somehow futuristic tone, we note that with the generation of non-Abelian gauge fields on an atomic gas, one will have at hand matter with intriguing topological charac-teristics. A possible application is the simulation of topologi-cal insulators with neutral atoms [see, e.g., Wu (2008), Goldman *et al.* (2010), and Stanescu, Galitski, and Das Sarma (2010)]. Another intriguing perspective could be to-pological quantum computing (Das Sarma, Freedman, and Nayak, 2006). In this respect the artificial gauge fields pro-vide a different scenario compared to the anticipated emer-gent non-Abelian excitations in, for instance, fractional quantum Hall systems. With artificially created gauge poten-tials the pseudospin is effectively turned into a non-Abelian anyon, since two pseudospins which swap places will be represented by different final states depending on whether they were interchanged clockwise or counterclockwise. Such effects may provide an atomic building block for fault toler-ant topological quantum computing.

ACKNOWLEDGMENTS

Note added in proof.—Since the completion of this review, two experimental realizations of an artificial gauge potential leading to a nonzero magnetic flux through the unit cell of an optical lattice have been reported (Aidelsburger *et al.*, 2011; Struck *et al.*, 2011).

REFERENCES

Aharonov, Y., and D. Bohm, 1959, Phys. Rev. **115**, 485.

Aharonov, Y., and A. Stern, 1992, Phys. Rev. Lett. **69**, 3593.

Aidelsburger, M., M. Atala, S. Nascimbène, S. Trotzky, Y.-A. Chen, and I. Bloch, 2011, arXiv:1110.5314.

Andersen, M. F., C. Ryu, P. Cladé, V. Natarajan, A. Vaziri, K. Helmerson, and W. D. Phillips, 2006, Phys. Rev. Lett. **97**, 170406.

Arimondo, E., 1996, in *Progress in Optics*, edited by E. Wolf (Elsevier, New York), Vol. 35, p. 259.

Ashcroft, N. W., and N. D. Mermin, 1976, *Solid State Physics* (Holt, Rinehardt and Winston, New York).

Aspect, A., E. Arimondo, R. Kaiser, N. Vansteenkiste, and C. Cohen-Tannoudji, 1988, Phys. Rev. Lett. **61**, 826.

Bergmann, K., H. Theuer, and B. W. Shore, 1998, Rev. Mod. Phys. **70**, 1003.

Berry, M. V., 1984, Proc. R. Soc. A **392**, 45.

Berry, M. V., 1989, in *Geometric Phases in Physics*, edited by A. Shapere and F. Wilczek (World Scientific, Singapore), p. 7.

Bloch, I., J. Dalibard, and W. Zwerger, 2008, Rev. Mod. Phys. **80**, 885.

Blount, E. I., 1962, Phys. Rev. **126**, 1636.

Bohm, A., B. Kendrick, M. Loewe, and L. Boya, 1992, J. Math. Phys. (N.Y.) **33**, 977.

Bohm, A., A. Mostafazadeh, H. Koizumi, Q. Niu, and J. Zwanziger, 2003, *Geometric Phases in Quantum Systems* (Springer, Berlin).

Buluta, I., and F. Nori, 2009, Science **326**, 108.

Campbell, D. L., G. Juzeliūnas, and I. B. Spielman, 2011, arXiv:1102.3945.

Castro Neto, A. H., F. Guinea, N. M. R. Peres, K. S. Novoselov, and A. K. Geim, 2009, Rev. Mod. Phys. **81**, 109.

Cheianov, V. V., V. Fal'ko, and B. L. Altshuler, 2007, Science **315**, 1252.

Cheneau, M., S. P. Rath, T. Yefsah, K. J. Günter, G. Juzeliūnas, and J. Dalibard, 2008, Europhys. Lett. **83**, 60 001.

Cohen-Tannoudji, C., and J. Dupont-Roc, 1972, Phys. Rev. A **5**, 968.

Cohen-Tannoudji, C., J. Dupont-Roc, and G. Grynberg, 1992, *Atom-Photon Interactions* (Wiley, New York).

Cooper, N. R., 2008, Adv. Phys. **57**, 539.

Cooper, N. R., 2011, Phys. Rev. Lett. **106**, 175301.

Cooper, N. R., and J. Dalibard, 2011, Europhys. Lett. **95**, 66004.

Cooper, N. R., and Z. Hadzibabic, 2010, Phys. Rev. Lett. **104**, 030401.

Cserti, J., and G. David, 2006, Phys. Rev. B **74**, 172305.

Dargys, A., 2010, Superlattices Microstruct. **48**, 221.

Das Sarma, S., M. Freedman, and C. Nayak, 2006, Phys. Today **59**, 32.

Datta, S., and B. Das, 1990, Appl. Phys. Lett. **56**, 665.

Dresselhaus, G., 1955, Phys. Rev. **100**, 580.

Dudarev, A. M., R. B. Diener, I. Carusotto, and Q. Niu, 2004, Phys. Rev. Lett. **92**, 153005.

Dum, R., and M. Olshanii, 1996, Phys. Rev. Lett. **76**, 1788.

Dutta, S. K., B. K. Teo, and G. Raithel, 1999, Phys. Rev. Lett. **83**, 1934.

Eckardt, A., C. Weiss, and M. Holthaus, 2005, Phys. Rev. Lett. **95**, 260404.

Fert, A., 2008, Rev. Mod. Phys. **80**, 1517.

Fetter, A. L., 2009, Rev. Mod. Phys. **81**, 647.

Feynman, R. P., 1982, Int. J. Theor. Phys. **21**, 467.

Fleischhauer, M., A. Imamoglu, and J. P. Marangos, 2005, Rev. Mod. Phys. **77**, 633.

Gerbier, F., and J. Dalibard, 2010, New J. Phys. **12**, 033007.

Gerritsma, R., G. Kirchmair, F. Zähringer, E. Solano, R. Blatt, and C. F. Roos, 2010, Nature (London) **463**, 68.

Goldman, N., 2007, Europhys. Lett. **80**, 20 001.

Goldman, N., 2009, *Quantum Transport in Lattices Subjected to External Gauge Fields* (VDM Verlag, Saarbrücken, Germany).

Goldman, N., A. Kubasiak, A. Bermudez, P. Gaspard, M. Lewenstein, and M. A. Martin-Delgado, 2009a, Phys. Rev. Lett. **103**, 035301.

Goldman, N., A. Kubasiak, P. Gaspard, and M. Lewenstein, 2009b, Phys. Rev. A **79**, 023624.

Goldman, N., I. Satija, P. Nikolic, A. Bermudez, M. A. Martin-Delgado, M. Lewenstein, and I. B. Spielman, 2010, Phys. Rev. Lett. **105**, 255302.

Grimm, R., M. Weidemüller, and Y. B. Ovchinnikov, 2000, Adv. At. Mol. Opt. Phys. **42**, 95.

Grünberg, P. A., 2008, Rev. Mod. Phys. **80**, 1531.

Günter, K. J., M. Cheneau, T. Yefsah, S. P. Rath, and J. Dalibard, 2009, Phys. Rev. A **79**, 011604.

Hadzibabic, Z., 2011 (private communication).

Harper, P. G., 1955, Proc. Phys. Soc. London Sect. A **68**, 874.

Harris, S., 1997, Phys. Today **50**, 36.

Hatsugai, Y., and M. Kohmoto, 1990, Phys. Rev. B **42**, 8282.

Hofstadter, D. R., 1976, Phys. Rev. B **14**, 2239.

Horváthy, P. A., 1986, Phys. Rev. D **33**, 407.

Hou, J.-M., W.-X. Yang, and X.-J. Liu, 2009, Phys. Rev. A **79**, 043621.

Jackiw, R., 1988, Comments At. Mol. Phys. **21**, 71.

Jacob, A., P. Öhberg, G. Juzeliūnas, and L. Santos, 2007, Appl. Phys. B **89**, 439.

Jaksch, D., and P. Zoller, 2003, New J. Phys. **5**, 56.

Johne, R., I. A. Shelykh, D. D. Solnyshkov, and G. Malpuech, 2010, Phys. Rev. B **81**, 125327.

Juzeliūnas, G., and P. Öhberg, 2004, Phys. Rev. Lett. **93**, 033602.

Juzeliūnas, G., P. Öhberg, J. Ruseckas, and A. Klein, 2005, Phys. Rev. A **71**, 053614.

Juzeliūnas, G., J. Ruseckas, and J. Dalibard, 2010, Phys. Rev. A **81**, 053403.

Juzeliūnas, G., J. Ruseckas, A. Jacob, L. Santos, and P. Öhberg, 2008, Phys. Rev. Lett. **100**, 200405.

Juzeliūnas, G., J. Ruseckas, M. Lindberg, L. Santos, and P. Öhberg, 2008, Phys. Rev. A **77**, 011802(R).

Juzeliūnas, G., J. Ruseckas, and P. Öhberg, 2005, J. Phys. B **38**, 4171.

Juzeliūnas, G., J. Ruseckas, P. Öhberg, and M. Fleischhauer, 2006, Phys. Rev. A **73**, 025602.

Katsnelson, M. I., K. S. Novoselov, and A. K. Geim, 2006, Nature Phys. **2**, 620.

Klein, A., and D. Jaksch, 2009, Europhys. Lett. **85**, 13 001.

Kohmoto, M., 1989, Phys. Rev. B **39**, 11 943.

Kolovsky, A. R., 2011, Europhys. Lett. **93**, 20 003.

Koo, H. C., J. H. Kwon, J. Eom, J. Chang, S. H. Han, and M. Johnson, 2009, Science **325**, 1515.

Král, P., I. Thanopulos, and M. Shapiro, 2007, Rev. Mod. Phys. **79**, 53.

Lamata, L., J. Leon, T. Schatz, and E. Solano, 2007, Phys. Rev. Lett. **98**, 253005.

Larson, J., J.-P. Martikainen, and A. Collin, 2010, Phys. Rev. A **82**, 043620.

Larson, J., and E. Sjöqvist, 2009, Phys. Rev. A **79**, 043627.

Lewenstein, M., A. Sanpera, V. Ahufinger, B. Damski, A. S. De, and U. Sen, 2007, Adv. Phys. **56**, 243.

Li, Y., C. Bruder, and C. P. Sun, 2007, Phys. Rev. Lett. **99**, 130403.

Lignier, H., C. Sias, D. Ciampini, Y. Singh, A. Zenesini, O. Morsch, and E. Arimondo, 2007, Phys. Rev. Lett. **99**, 220403.

Lim, L.-K., C. M. Smith, and A. Hemmerich, 2008, Phys. Rev. Lett. **100**, 130402.

Lin, Y., K. Jiménez-García, and I. Spielman, 2011, Nature (London) **471**, 83.

Lin, Y. J., R. L. Compton, A. R. Perry, W. D. Phillips, J. V. Porto, and I. B. Spielman, 2009, Phys. Rev. Lett. **102**, 130401.

Lin, Y.-J., R. L. Compton, K. Jiménez-García, J. V. Porto, and I. B. Spielman, 2009, Nature (London) **462**, 628.

Littlejohn, R. G., and S. Weigert, 1993, Phys. Rev. A **48**, 924.

Lukin, M. D., 2003, Rev. Mod. Phys. **75**, 457.

Luttinger, J. M., 1951, Phys. Rev. **84**, 814.

Mandel, O., M. Greiner, A. Widera, T. Rom, T. W. Hänsch, and I. Bloch, 2003, Phys. Rev. Lett. **91**, 010407.

Mead, C. A., 1992, Rev. Mod. Phys. **64**, 51.

Mead, C. A., and D. G. Truhlar, 1979, J. Chem. Phys. **70**, 2284.

Merkl, M., F. E. Zimmer, G. Juzeliūnas, and P. Öhberg, 2008, Europhys. Lett. **83**, 54002.

Messiah, A., 1961a, *Quantum Mechanics* (North-Holland, Amsterdam), Vol. II, Chap. XV, Sec. 19.

Messiah, A., 1961b, *Quantum Mechanics* (North-Holland, Amsterdam), Vol. II, Chap. XVII, Sec. 13.

Möller, G., and N. R. Cooper, 2009, Phys. Rev. Lett. **103**, 105303.

Möller, G., and N. R. Cooper, 2010, Phys. Rev. A **82**, 063625.

Moody, J., A. Shapere, and F. Wilczek, 1986, Phys. Rev. Lett. **56**, 893.

Moody, J., A. Shapere, and F. Wilczek, 1989, in *Geometric Phases in Physics*, edited by A. Shapere and F. Wilczek (World Scientific, Singapore), p. 160.

Mueller, E. J., 2004, Phys. Rev. A **70**, 041603.

Nenciu, G., 1991, Rev. Mod. Phys. **63**, 91.

Osterloh, K., M. Baig, L. Santos, P. Zoller, and M. Lewenstein, 2005, Phys. Rev. Lett. **95**, 010403.

Pietilä, V., and M. Möttönen, 2009, Phys. Rev. Lett. **102**, 080403.

Polak, T. P., and T. K. Kopeć, 2009, Phys. Rev. A **79**, 063629.

Rashba, E. I., 1960, Sov. Phys. Solid State **2**, 1109.

Ruostekoski, J., 2009, Phys. Rev. Lett. **103**, 080406.

Ruostekoski, J., G. V. Dunne, and J. Javanainen, 2002, Phys. Rev. Lett. **88**, 180401.

Ruseckas, J., G. Juzeliūnas, P. Öhberg, and M. Fleischhauer, 2005, Phys. Rev. Lett. **95**, 010404.

Rusin, T. M., and W. Zawadzki, 2009, Phys. Rev. B **80**, 045416.

Rusin, T. M., and W. Zawadzki, 2010, Phys. Rev. D **82**, 125031.

Satija, I. I., D. C. Dakin, J. Y. Vaishnav, and C. W. Clark, 2008, Phys. Rev. A **77**, 043410.

Schliemann, J., J. C. Egues, and D. Loss, 2003, Phys. Rev. Lett. **90**, 146801.

Schliemann, J., D. Loss, and R. M. Westervelt, 2006, Phys. Rev. B **73**, 085323.

Smith, F. T., 1969, Phys. Rev. **179**, 111.

Song, J.-J., and B. A. Foreman, 2009, Phys. Rev. A **80**, 045602.

Sørensen, A. S., E. Demler, and M. D. Lukin, 2005, Phys. Rev. Lett. **94**, 086803.

Spielman, I. B., 2009, Phys. Rev. A **79**, 063613.

Stanescu, T., B. Anderson, and V. Galitski, 2008, Phys. Rev. A **78**, 023616.

Stanescu, T. D., V. Galitski, and S. Das Sarma, 2010, Phys. Rev. A **82**, 013608.

Stanescu, T. D., C. Zhang, and V. Galitski, 2007, Phys. Rev. Lett. **99**, 110403.

Struck, J., C. Ölschläger, R. Le Targat, P. Soltan-Panahi, A. Eckardt, M. Lewenstein, P. Windpassinger, and K. Sengstock, 2011, Science **333**, 996.

Teodorescu, V., and R. Winkler, 2009, Phys. Rev. B **80**, 041311(R).

Thouless, D. J., M. Kohmoto, M. P. Nightingale, and M. den Nijs, 1982, Phys. Rev. Lett. **49**, 405.

Tinkham, M., 1996, *Introduction to Superconductivity* (McGraw-Hill, New York).

Tung, S., V. Schweikhard, and E. A. Cornell, 2006, Phys. Rev. Lett. **97**, 240402.

Unanyan, R. G., M. Fleischhauer, B. W. Shore, and K. Bergmann, 1998, Opt. Commun. **155**, 144.

Unanyan, R. G., B. W. Shore, and K. Bergmann, 1999, Phys. Rev. A **59**, 2910.

Vaishnav, J. Y., and C. W. Clark, 2008, Phys. Rev. Lett. **100**, 153002.

Vaishnav, J. Y., J. Ruseckas, C. W. Clark, and G. Juzeliūnas, 2008, Phys. Rev. Lett. **101**, 265302.

Visser, P. M., and G. Nienhuis, 1998, Phys. Rev. A **57**, 4581.

Vitanov, N. V., M. Fleischhauer, B. W. Shore, and K. Bergmann, 2001, Adv. At. Mol. Opt. Phys. **46**, 55.

Wang, C., C. Gao, C.-M. Jian, and H. Zhai, 2010, Phys. Rev. Lett. **105**, 160403.

Wang, Y.-F., and C.-D. Gong, 2006, Phys. Rev. B **74**, 193301.

Weigert, S., and R. G. Littlejohn, 1993, Phys. Rev. A **47**, 3506.

Wilczek, F., and A. Zee, 1984, Phys. Rev. Lett. **52**, 2111.

Williams, R. A., S. Al-Assam, and C. J. Foot, 2010, Phys. Rev. Lett. **104**, 050404.

Winkler, R., 2003, *Spin-Orbit Coupling Effects in Two-Dimensional Electron and Hole Systems* (Springer, Berlin).

Wu, C., 2008, Phys. Rev. Lett. **101**, 186807.

Xiao, D., M.-C. Chang, and Q. Niu, 2010, Rev. Mod. Phys. **82**, 1959.

Ye, J., H. J. Kimble, and H. Katori, 2008, Science **320**, 1734.

Yi, W., A. Daley, G. Pupillo, and P. Zoller, 2008, New J. Phys. **10**, 073015.

Yip, S.-K., 2011, Phys. Rev. A **83**, 043616.

Zee, A., 1988, Phys. Rev. A **38**, 1.

Zhang, P., Y. Li, and C. P. Sun, 2005, Eur. Phys. J. D **36**, 229.

Zhang, Q., J. Gong, and C. Oh, 2010, Ann. Phys. (N.Y.) **325**, 1219.

Zhou, Xiang-Fa, Jing Zhou, and Congjun Wu, 2011, Chin. Phys. Lett. **28**, 097102.

Zhu, S.-L., H. Fu, C.-J. Wu, S.-C. Zhang, and L.-M. Duan, 2006, Phys. Rev. Lett. **97**, 240401.

Zutic, I., J. Fabian, and S. Das Sarma, 2004, Rev. Mod. Phys. **76**, 323.

Zygelman, B., 1987, Phys. Lett. A **125**, 476.

Zygelman, B., 1990, Phys. Rev. Lett. **64**, 256.